Aeroacoustic optimization of a supersonic business jet

Andrea Minelli, Gérald Carrier, Jean-Antoine Desideri, Régis Duvigneau, Itham Salah El Din

Aeroacoustic optimization of a supersonic business jet

Andrea Minelli — Gérald Carrier — Jean-Antoine Désidéri

Regis Duvigneau — Itham Salah el Din

N° 7477

December 2010

R apport de recherche

Aeroacoustic optimization of a supersonic business jet

Andrea Minelli[*], Gérald Carrier[†], Jean-Antoine Désidéri[‡]
Regis Duvigneau[§], Itham Salah el Din[¶]

Abstract: A multiobjective optimization has been developed for the design of the fuselage of a supersonic business jet. The attention is focused on the coupling between the CFD solver (Num3sis) developed at INRIA and the acoustic propagation code TRAPS in use at ONERA. The accuracy of the propagation prediction over the entire domain is fundamental for obtaining a valuable solution. In order to achieve this objective an iterative procedure for unstructured mesh adaptation is developed. Mesh adaptation has the potential to reduce the computational time increasing the density of the mesh only where required.

After a brief introduction of the different tools required to solve the problem in analysis, the optimization is carried out in a hybrid process in which an evolutionary strategy (ES) is used first (exploration), and a gradient based method second for improve the accuracy (exploitation). The Pareto optimal curve is evaluated using the Pareto Archive Evolutionary Strategy[17] and with a classical Adapted Weighted Sum method[18] in order to compare the final results.

This design methodology has the ability to generate non intuitive configuration that do not rely on the engineer's experience. Combining CAD modeling, CFD, acoustic propagation analysis and shape multicriterion optimization enhance the potential of investigation of such a complex physical phenomenon.

Key-words: Shape optimisation, unstructured mesh, mesh adaptation, sonic boom reduction, hybrid algorithm, Evolutionary Strategies, Weighted sum

[*] INRIA Sophia Antipolis. Email: Andrea.Minelli@sophia.inria.fr
[†] ONERA Meudon. Email: Gerald.Carrier@onera.fr
[‡] INRIA Sophia Antipolis. Email: Jean-Antoine.Desideri@sophia.inria.fr
[§] INRIA Sophia Antipolis. Email: Regis.Duvigneau@sophia.inria.fr
[¶] ONERA Meudon. Email: itham.Salah_el_din@onera.fr

Optimisation aéroacoustique
d'un avion d'affaires supersonique

Résumé : On a développé un outil d'optimisation multiobjectif pour la conception du fuselage d'un avion d'affaires supersonique. L'effort est centré sur le couplage du solveur CFD Num3sis de l'INRIA et le code TRAPS en usage à l'ONERA en analyse de propagation acoustique. La précision du calcul de propagation du signal acoustique dans tout le domaine est essentielle à une simulation pertinente. A cette fin, une procédure itérative permet l'adaptation du maillage non structuré. L'adaptation du maillage permet à coût réduit d'augmenter la précision du calcul en restreignant aux zones critiques de l'écoulement le raffinement du maillage.

Après une brève introduction des différents outils d'analyse, l'optimisation est faite par une procédure hybride dans laquelle on applique d'abord une stratégie évolutionnaire (ES) pour l'exploration de l'espace, puis une méthode de gradient pour affiner le résultat (exploitation). Le front de Pareto est identifié en utilisant la Stratégie Evolutionnaire d'Archive de Pareto (*Pareto Archive Evolutionary Strategy [17]*) et la méthode classique de critères pondérés (*Adapted Weighted Sum Method* [18]), et les résultats sont comparés.

Cette méthodologie de conception permet de générer des configurations non intuitives ne s'appuyant pas sur l'expérience de l'ingénieur. La combinaison des outils de modélisation géométrique CAD, de CFD, d'analyse de propagation d'onde acoustique, et d'optimisation de forme multicritère permet d'augmenter le potentiel d'investigation des écoulements physiquement complexes.

Mots-clés : Optimisation de forme, maillage non structurè, adaptation de maillage, redùction du bang sonique, algorithme hybride, Stratégie Evolutionnaire, critères pondérés

Contents

1 Introduction

This research aims to develop an overview of the approach and of the algorithms required in the analysis of a shape optimization problem for a supersonic business jet.

In particular the research aims to consider the sonic boom minimization in a multicriteria optimisation loop while maintaining global aerodynamic performance. The sonic boom is a physical phenomenon related to the motion of a body in the atmosphere at a speed exceeding the local speed of sound. When this happens shock waves are generated. These ones consist in surfaces of discontinuity called Mach cones for thermodynamic quantities such as pressure and density and for the relative velocity of the atmosphere. Usually these shock waves evolve during the propagation along the atmosphere creating N-shaped waves when they reach the ground, resulting from the coalescence of the shock waves caused by nonlinear effects.

In order to evaluate these effects the extrapolation of the pressure field around the airplane is used as initial condition for the ground propagation. In this way, it is possible to evaluate the sonic boom signature and define a valuable criteria for the algorithm. This procedure aims to rebuild a Whitham function equivalent, at long distance, to the pressure perturbation generated by the aircraft. The technique involved in the acoustic propagation is based on the ray-tracing method[14] that will be introduced later.

The minimization of sonic boom is one of the main aspect that influence the design of advanced supersonic transport, environmental assesment of launcher vehicles and is a valuable criteria for environmental assesment of military aircraft operations. In addition the commercial supersonic flights overlands are banned with international laws. Despite these aspects, nowadays convencional shape for reducing the boom phenomenon are not defined. NASA admitted that commercial supersonic transport cannot flourish without a revolutionary design. In fact in the market perspective [20] appears evident that at the beginning only small supersonic business jet operating at Mach 1.8-2.0 could have a profitable market. In addition it implies technological challenges that can be affordable. Most of the study efforts are focused on the definition of a baseline configuration for a low boom SSBJ. Sonic boom can be only reduced, because it is impossible to avoid a lift contribution [7].

1.1 The sonic boom phenomenon

An airplane moving in the atmosphere creates over and underpressure areas and when it moves at a supersonic speed, the acoustic waves are focused in a conic space. The noise emited from the source is limited inside this zone. The Mach cone has origin at the vertex of the aircraft nose and it has an angle of 2α such as $\sin\alpha = c/a = M^{-1}$ where c, a and M are the sound speed, the aircraft velocity and the Mach number.

Every part of the airplane create its own Mach cone. When these acoustic waves propagate in a non uniform atmosphere the different temperature can accelerate or decelerate the waves. Considering that the propagation is developed for at least 10 km, these waves tend to coalesce in a characteristic N-shaped wave. The signal that reaches the ground shows two strong shocks at its beginning and at end that causes a high perceived loudness PldB.

From an environmental point of view there are several possible impact on structures and human beings as a function of the magnitude of the disturbance that reaches the ground:

Sonic Boom overpressure [Pa]	Effects
< 48	No structural damages, Noise
48 - 96	Disturbance to people
96 - 240	Small and rare structural damages
530	Structural damages for recent buildings
34500	Rupture of the eardrum

Concorde, the only supersonic civil airplane has ever flown, flying at Mach 2 at an altitude of 52000 ft produced an overpressure of 90 Pa. This value was increased during the manouvers, at a low altitude or due to different atmospheric conditions, so it belongs to the range that produce disturbances to people and small structural damages. This is one of the reasons that led to the end of Concorde flights in November 2003.

One of the peculiar aspect of the phenomenon is the propagation through the atmosphere. Typical signature shapes evolve during the propagation as shown in figure 1. It is possible to identify three area in the analysis domain: near,mid
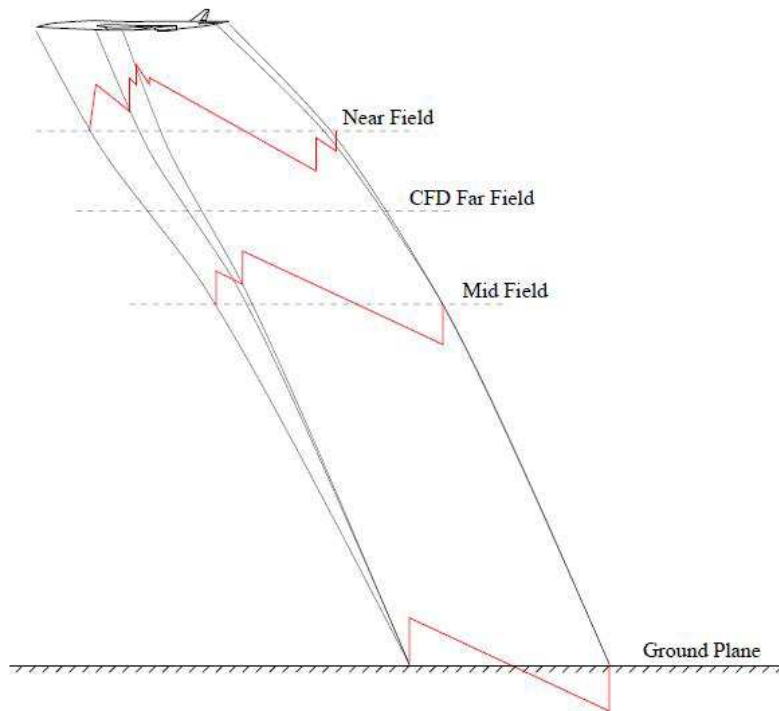

Figure 1: Sonic boom phenomenon

and far field. The near field have an extension approximatively equal to 2-3

fuselage length below it. In this zone the atmospheric gradient do not play an important role, and a linear approximation is sufficient for the description of the waves propagation. The mid field takes into account the flow from near field to hundreds characteristic lengths. In this region the propagation shows high non linear effects that in the far field creates the characteristic N-shape.

One of the main challenges is the difference of scale between the shock width that have magnitude of μm and the computational domain that is around 15 km for a SSBJ. Consider a 3D CFD computatation with Navier-Stokes or Euler equation over the entire domain is computationally too expensive for an accurate solution.

The solution commonly adopted is the propagation of the disturbances to the ground via simplified acoustic models. The simplest approach is based on the Witham theory(1952). The pressure field is translated into an equivalent one-dimensional F-function. This method takes into account second order non linear effects during the propagation through the atmosphere.

A more accurate method is based on the optic geometry. In particular is based on the ray-tracing technique for the ground propagation. In this way it is possible to consider more general ground signal instead of those provided with a simple F-function method and to consider real atmosphere models.

The strategy developed in literature applies 3D Euler equations in the near field and then the pressure field is propagated to the far field using an acoustic propagation code [15].

This process is validated with wind tunnel tests and in [11] it has been demonstrated that the numerical results are in agreement with the wind tunnel experiments.

1.2 Objectives and contents of this research

This work is a part of a greater scope with regard to the multicriteria shape optimization. In particular this research aims at the analysis of an aeroacoustic shape optimization. The first step required consists in the definion, development and verification of all the tools required in the problem analysis. Next step consists in the optimization with appropriate criteria. In this first part of the work the objective is the optimization of the fuselage nose of a SSBJ in order to minimize the sonic boom, maintaining good aerodynamic efficiency.

In the first sections the problem is defined in the aerodynamic and acoustic field. After the definition of the tools required for the optimization the results are presented.

2   CFD computation

This part aims to introduce briefly the problem from the fluid dynamics point of view in particular considering the computation algorithm.

The flow analysis is performed using the NUM3SIS flow solver developed at INRIA Sophia-Antipolis. This study is restricted to three-dimensional compressible flows governed by the laminar Navier-Stokes equations. Then, the state equations can be written in the conservative form :

$$\frac{\partial W}{\partial t} + \frac{\partial F_1(W)}{\partial x} + \frac{\partial F_2(W)}{\partial y} + \frac{\partial F_3(W)}{\partial z} = \frac{\partial G_1(W)}{\partial x} + \frac{\partial G_2(W)}{\partial y} + \frac{\partial G_3(W)}{\partial z} \quad (1)$$

where W are the conservative flow variables $(\rho, \rho u, \rho v, \rho w, E)$, with ρ the density, $\overrightarrow{U} = (u, v, w)$ the velocity vector and E the total energy per unit of volume. $\overrightarrow{F} = (F_1(W), F_2(W), F_3(W))$ is the vector of the convective fluxes and $\overrightarrow{G} = (G_1(W), G_2(W), G_3(W))$ the vector of the diffusive fluxes. The pressure p is obtained from the perfect gas state equation :

$$p = (\gamma - 1)(E - \frac{1}{2}\rho\|\overrightarrow{U}\|^2) \quad (2)$$

where $\gamma = 1.4$ is the ratio of the specific heat coefficients.

Provided that the flow domain Ω is discretized by a tetrahedrization $\mathcal{T}_h$, a discretization of equation (1) at the mesh node s_i is obtained by integrating (1) over the volume C_i, that is built around the node s_i by joining barycenters of the tetrahedra and triangles containing s_i and midpoints of the edges adjacent to s_i :

$$Vol_i \frac{\partial W_i}{\partial t} + \sum_{j \in N(i)} \Phi(W_i, W_j, \overrightarrow{\sigma}_{ij}) = \sum_{k \in E(i)} \Psi_k \quad (3)$$

where W_i represents the cell averaged state and Vol_i the volume of the cell C_i (see figure 2). $N(i)$ is the set of the neighboring nodes and $E(i)$ the set of the neighboring tetrahedra. $\Phi(W_i, W_j, \overrightarrow{\sigma}_{ij})$ is an approximation of the integral of the convective fluxes over the boundary ∂C_{ij} between C_i and C_j, which depends on W_i, W_j and $\overrightarrow{\sigma}_{ij}$ the integral of a unit normal vector over ∂C_{ij}. The convective fluxes are evaluated using upwinding, according to the approximate Riemann solver HLLC [5]. Ψ_k is an approximation of the diffusive fluxes integrated on the part of the control surface located in the tetrahedron k, according to a classical P1 description of the flow fields. A high order upwind scheme is obtained by reconstructing the physical variables at the midpoint of $[s_i s_j]$ using W_i, W_j and the gradient ∇W in the upwind tetrahedron (β-scheme) , before the fluxes are evaluated. In order to avoid spurious oscillations of the solution in the vicinity of the shock, a slope limitation procedure using the Barth-Jespersen limiter[4] is introduced.

An implicit pseudo-time stepping procedure is used for the time integration of (3). A classical three-step backward scheme ensures a second-order accurate discretization of the physical time term. A first-order backward scheme is employed for the pseudo-time integration. The linearization of the numerical fluxes
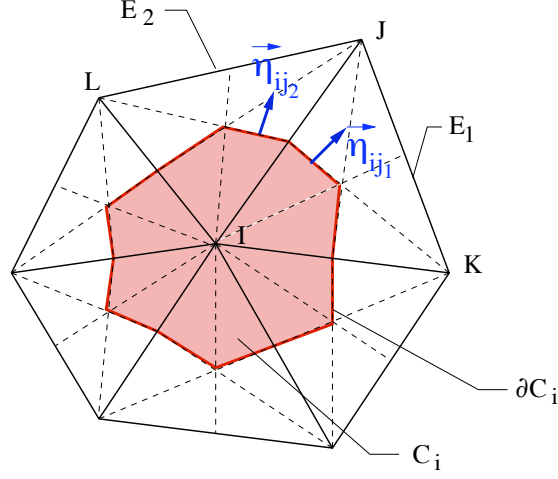
Figure 2: Exemple of control cell

provides the following integration scheme :

$$\left(\left(\frac{Vol_i}{\Delta t} + \frac{Vol_i}{\Delta \tau} \right) Id + J_i^p \right) \delta W_i^{p+1} = - \sum_{j \in N(i)} \Phi_{ij}^p + \sum_{k \in E(i)} \Psi_k^p - \frac{3}{2} \frac{Vol_i}{\Delta t} \delta W_i^n + \frac{1}{2} \frac{Vol_i}{\Delta t} \delta W_i^{n-1}$$

$$(4)$$

with :

$$\delta W_i^{p+1} = (W_i^{n+1})^{p+1} - (W_i^{n+1})^p \quad (5)$$
$$\delta W_i^n = (W_i^{n+1})^p - W_i^n \quad (6)$$
$$\delta W_i^{n-1} = W_i^n - W_i^{n-1} \quad (7)$$

J_i^p is the Jacobian matrix of the numerical fluxes. $\Delta \tau$ is the pseudo-time step. For the Jacobian computation, we employ the first-order flux of Rusanov, yielding a matrix-free resolution scheme based on a point-Jacobi method. The right hand side of (4) is evaluated using high order approximations. The resulting integration scheme provides a second-order solution in space and time.

The flow solver is designed for large-scale parallel computing, on the basis of a domain decomposition strategy relying on the MPI library.

3 Mesh Adaptation

In the analysis of a sonic boom problem there are some aspects that influence the accuracy of the ground signature: mesh resolution, artificial dissipation and acoustic propagation algorithm.

The adaptation of an unstructured mesh improves the accuracy of the solution obtained and permits to capture the physical phenomena in analysis. These aspects are also linked with the reduction of the computational time with a smart reduction of the elements number and in this way degree of freedom. The approach used in this research instead of a adaptation of the initial mesh regenerate a new completely adapted mesh. This adaptation process takes the information from the previous mesh, and in particular information related to the physical phenomena in analysis. The most popular criteria for mesh refinement and adaptation are based on the gradient. The first step is a method to evaluate these quantities in order to have a valuable information for the following adaptation.

3.1 Least square method to evaluate the flow derivatives

In order to identify the criteria used in the mesh regeneration and adaptation it is necessary to evaluate the Hessian matrix of a characteristic flow variable Φ. This approach belongs to the Hessian based error estimation technique. Following the same strategy developed in [12] for an unstructured bi-dimensional mesh we upgrade this approach considering a three dimensional unstructured mesh.
The second order Taylor expansion of a generic flow variable around the node P (x_P, y_P, z_P) can be written as:

$$
\begin{aligned}
\phi(x,y,z) \quad = \quad & \phi(x_P, y_P, z_P) + (x - x_P)\phi_x + (y - y_P)\phi_y + (z - z_P)\phi_z + \\
& + (x - x_P)(y - y_P)\phi_{xy} + (x - x_P)(z - z_P)\phi_{xz} + (y - y_P)(z - z_P)\phi_{yz} + \\
& + \tfrac{1}{2}(x - x_P)^2\phi_{xx} + \tfrac{1}{2}(y - y_P)^2\phi_{yy} + \tfrac{1}{2}(z - z_P)^2\phi_{zz}
\end{aligned}
\tag{8}
$$

It is possible to define an array $\mathbf{x}_\phi$ that contains all the unknowns variables:

$$
\mathbf{x}_\phi = \{\phi, \phi_x, \phi_y, \phi_z, \phi_{xy}, \phi_{xz}, \phi_{yz}, \phi_{xx}, \phi_{yy}, \phi_{zz}\}^T
\tag{9}
$$

Their values are determined by matching with the least square approach the value of the Taylor expansion to that of the flow variable at a set of points that belongs to a patch $\mathcal{P}$ surrounding the node P.

This corresponds to the evaluation of a overdetermined system of equations:

$$
\phi_N = \mathbf{B}^T \mathbf{x}_\phi
\tag{10}
$$

where $\phi_N = (x_N, y_N)$ and N belongs to the patch $\mathcal{P}$ and $\mathbf{B}$ is defined as

$$
\mathbf{B} = \{1, (x - x_P), ..., (x - x_P)(y - y_P), ..., 1/2(z - z_P)^2\}
$$

.

To evaluate the unknowns a minimization problem of the square distance between the Taylor expansion and the value of the variable at node N is defined. The functional cost to be minimized is

$$\min J(\mathbf{x}_\phi) = \frac{1}{2} \sum_{N \in \mathcal{P}} \left(\mathbf{B}^T \mathbf{x}_\phi - \phi_N \right)^2 \tag{11}$$

The stationary condition of eq.11 with respect to the unknowns is defined by the following linear system

$$\sum_{N \in \mathcal{P}} \mathbf{B}\mathbf{B}^T \mathbf{x}_\phi = \sum_{N \in \mathcal{P}} \mathbf{B}\phi_N \tag{12}$$

This condition is also sufficient to determine the minimum because the matrix $\mathbf{B}\mathbf{B}^T$ is symmetric and positive definite. An accurate assessment of the derivatives is closely linked to the choice of an appropriate stencil. The minimum number of nodes because the problem is well placed and then the condition number of the matrix is nonzero is equal to the number of unknowns. The patch is created considering the nodes belonging to the tetrahedron that share the node $P(x_P, y_P, z_P)$.

In figure 3 the patch around a mesh node is shown. The number of elements that belong to this patch is limited. This solution could be adequate inside the domain where the mesh is sufficiently fine, but it is a poor approach in the boundary zones.
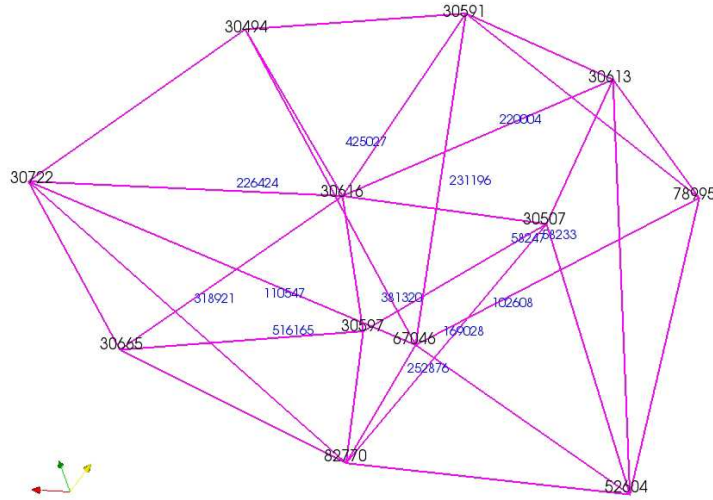

Figure 3: First stencil for interpolation around node 30616. In black nodes label, in blue cells ID

In fact, in these areas the number of patch nodes could be more than the necessary condition, but if many of the nodes are coplanar they do not provide an accurate information. Evidence of this aspect is provided by the condition number of $\mathbf{B}\mathbf{B}^T$ evaluate at a boundary node, that it is orders of magnitude lower then nodes where the solution is considered accurate.
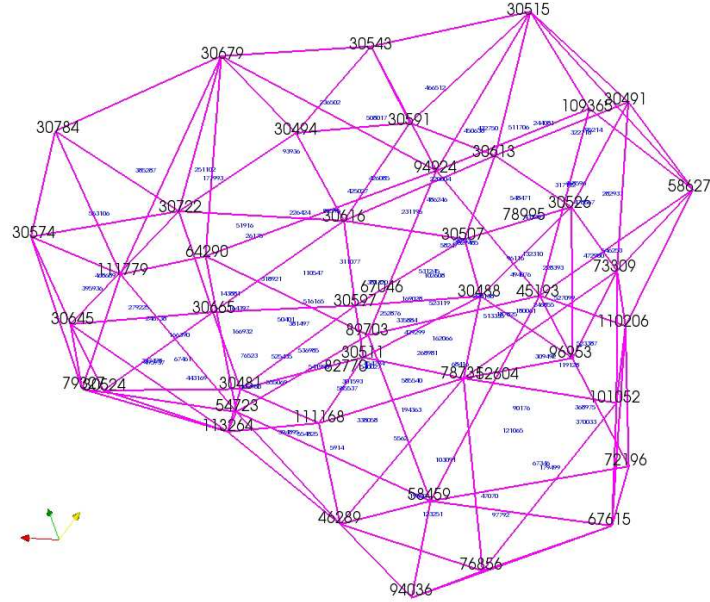
Figure 4: Improved stencil for interpolation around node 30616. In black nodes label, in blue cells ID

Using a symmetric plane in the simulation lead to an inaccurate solution in the critical part of the domain, because the fuselage belongs to the boundary. For this reason we chose to adopt an extended stencil that takes into account the so-called neighbors of neighbors node. The patch $\mathcal{P}$ in the vicinity of the node P is enlarged by adding the patches of all the node which belongs to $\mathcal{P}$. It will thus increased the number of points belonging to the patch and this avoiding the problem of coplanar nodes.

The result is a good quality solution, showing an high condition number of $\mathbf{BB}^T$ and never equal to zero. Figure 4 shows the improved stencil. The number of nodes and elements is increased from the simple stencil over the same node.

3.2 Criteria for mesh adaptation

In this section we want to make a first analysis about the selection of the criteria to be used for the generation of a new adapted mesh. In order to identify a valuable criteria I we consider the problem analyzed in [16]. The problem consists in the analysis of a double shock reflection over an oblique stationary contact discontinuity. The starting point consists in the evaluation of the derivatives of a characteristic flow variable from the solution of a coarse mesh.

Figure 6 shows the pressure field with a mesh of 19050 elements. The information appears to be too diffused in the shock zone, and the shock line is not evaluated with an adequate accuracy. It is interesting to evaluate the pressure and its derivatives over a line along the axis of the channel. The second derivatives is high just before and after the shock, while the first derivative reach its maximum in the shock area. Considering only one information appears to be inaccurate. In fact considering only a criteria based on P_x the shock is well
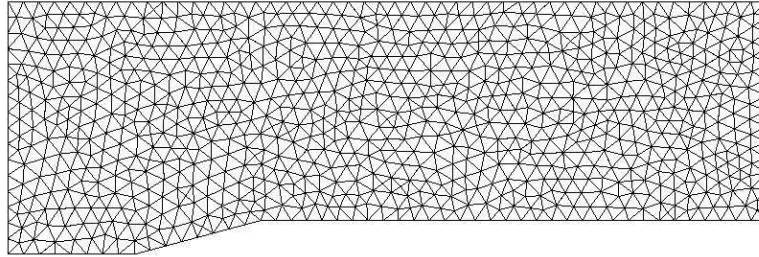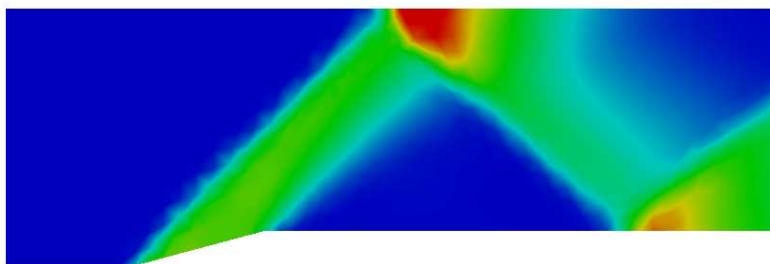
Figure 5: Channel initial mesh of 19050 elements

Figure 6: Pressure field with an initial mesh of 19050 elements

described, but in the neighborhood the information is too diffused, otherwise a criteria based only on P_{xx} do not describe in an accurate way the shock. The solution proposed in this work is a linear combination defined as:

$$I = w_1 P_x + w_2 P_{xx} \tag{13}$$
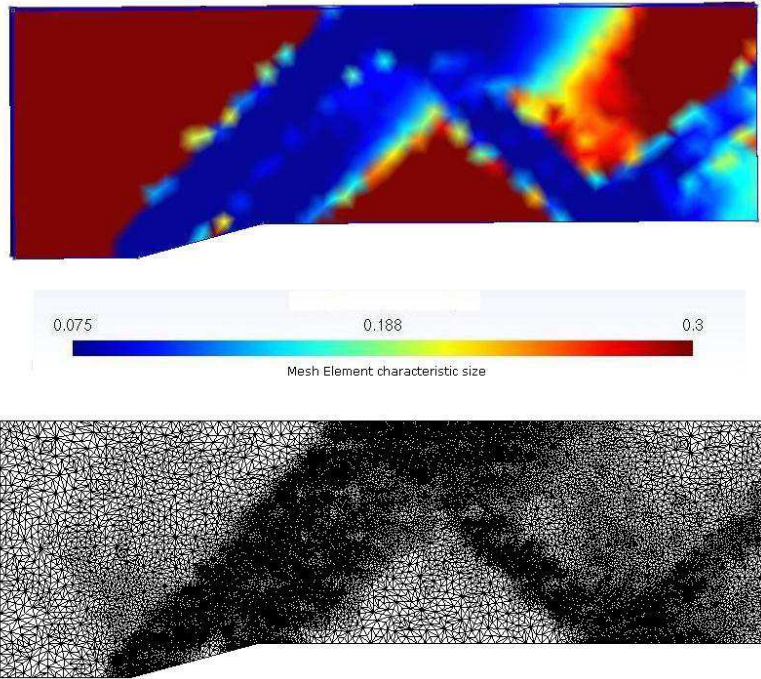
where w_1 and w_2 are weights.

Figure 7: Characteristic size of the elements in the adapted mesh and adapted mesh of 112825 elements

Figure 7 shows the size of the elements in the new mesh. The mesh is refined mainly in the shock areas, while the other elements that belongs to other areas maintain the characteristic size of the old mesh.

The pressure field evaluated with the new adapted mesh is shown in figure 8. The shock appears to be well defined and there are no diffusion due to the mesh quality. The shock reflection zone where the overpressure reaches its maximum increases its extension. These aspect is due to an accurate propagation of the information inside the domain.

Mesh adaptation is a key step in order to avoid bad quality solution. This procedure could be computationally expensive, a compromise between computational efforts and the accuracy of the solution is required.

In the aero-acoustic optimization an accurate CFD computation is also required for the acoustic propagation in the far field. An improvement can be reached maintaining an equal number of elements between the initial and the adapted mesh or coarsening the mesh in the not critical areas for the analysis. Despite this [10] states that for a stationary problem there are no significant
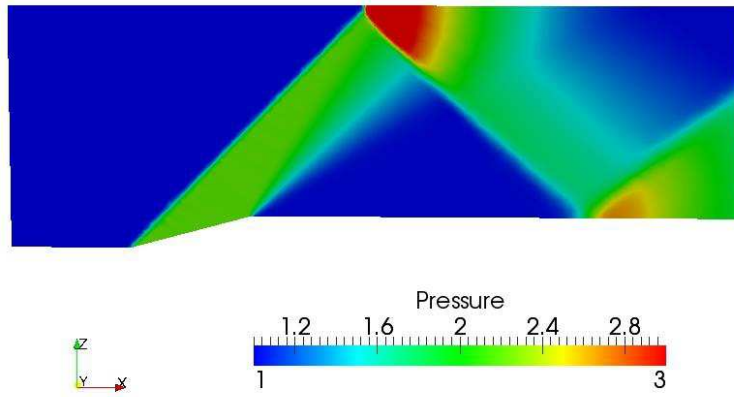
Figure 8: Pressure field with an adapted mesh of 112825 elements

computational saving in coarsening the mesh. Further research in mesh adaptation will focus on this topic.

4   Acoustic propagation

The CFD calculation is used to evaluate the disturbance by the supersonic motion of the aircraft. The aircraft pressure perturbations must be propagated through the atmosphere in order to evaluate the pressure signature in the far field. At this stage nonlinear distortions occur due to non-uniformity of the means in which the wave propagates. These non-uniformity directly affect the speed of propagation of disturbances that is different at a local level. In this way during propagation, the disturbances tend to coalesce and form a shock with higher intensity. The nonlinear distortion can be treated considering the nonlinear acoustic theory under the assumptions of low-intensity disturbances.

The propagation through a non-uniform atmosphere is described using the acoustic geometry[14]. This theory is used under the hypothesis that the ratio between the disturbance scale and the propagation scale is small enough.

Considering these theories the attention is focused on the signal emitted from the source. In particular the ray are emitted from every part of the airplane.

The pressure field evaluated with CFD has to be extracted over a cylinder aligned with the flow direction. In this way it is possible to use a multipole decomposition method [15] that from the near field pressure signature on the cylinder, it allows to generate the Whitham function equivalent to the pressure perturbation generated by the aircraft on the ground.

The propagation is computed using an acoustic propagation code, TRAPS. It uses a ray-tracing approach in order to take into account the refraction phenomena occurring during the propagation through a stratified non-uniform atmosphere. Using the ray-tracing method it is also possible to define a relationship between the Whitham function and the variation of the pressure on the ground. This one is the parameter necessary for the following optimization using an acoustic criteria.

This program allows us to consider aircraft performing maneuvers, acceleration and deceleration, according to a trajectory specified by the user [21]. The trajectory is defined in an Inertial Navigation System located on the ground and it consists in the airplane height and in the position on the altitude plane sampled at time intervals.

The atmosphere is considered steady and modeled as stratified vertically and horizontally uniform. It is also possible to consider the presence of wind during the flying path, but this aspect is not considered at this research step.

4.1   Extrapolation of the pressure field over a cylinder

In order to interpolate the pressure field over a cylinder two steps are essentially required:

1. Isolation of the tetrahedral element in the unstructured mesh which belongs to the structured cylinder grid node;

2. Evaluation of pressure on the nodes belonging to the structured cylinder grid by linear interpolation.

The first phase requires the identification of the internal volume of each tetrahedron. Every faces of a tetrahedron is identified by a plane

$$\pi : ax + by + cz + d = 0 \tag{14}$$

Considering a tetrahedron $\mathcal{T}$ formed by the planes $\pi_i, \pi_j, \pi_k, \pi_l$ with normal positive outward from the internal domain of the element, the volume of the tetrahedron is defined by the following inequalities: $\pi_n \leq 0$, with $n = i, j, k, l$

The next step of the algorithm requires the verification for each node of the structured grid which tetrahedron satisfy all necessary and sufficient conditions identified previously. If the point P considered respects the conditions $\pi_n^\tau(P) \leq 0$, with $n = i, j, k, l$, it belongs to the tetrahedron τ.

This operation can be extremely expensive in terms of computational times for unstructured grids consisting of a large number of elements. Various strategies can be identified in the future development and consist essentially in the parallelization of the elements research and / or using a smart search that uses knowledge about the problem geometry.

After the identification of the tetrahedral element it is necessary to evaluate the value of the characteristic variable at the node that belongs to the structured cylinder mesh.

The value of the pressure at point $\mathbf{r}$ located inside the tetrahedron could be written as a weighted sum of the values at the element nodes $\mathbf{r}_1, \mathbf{r}_2, \mathbf{r}_3, \mathbf{r}_4$ using the so-called barycentric coordinates.

$$p(\mathbf{r}) = \lambda_1 p(\mathbf{r}_1) + \lambda_2 p(\mathbf{r}_2) + \lambda_3 p(\mathbf{r}_3) + \lambda_4 p(\mathbf{r}_4) \tag{15}$$

with the constraint

$$\lambda_1 + \lambda_2 + \lambda_3 + \lambda_4 = 1 \tag{16}$$

Starting from the Cartesian coordinates of each node and using the barycentric coordinates the weights can be evaluated solving the linear system:

$$\mathbf{T} \cdot \lambda = \mathbf{r} - \mathbf{r}_4 \tag{17}$$

where

$$\mathbf{T} = \begin{pmatrix} x_1 - x_4 & x_2 - x_4 & x_3 - x_4 \\ y_1 - y_4 & y_2 - y_4 & y_3 - y_4 \\ z_1 - z_4 & z_2 - z_4 & z_3 - z_4 \end{pmatrix} \tag{18}$$

and $\lambda^T = \{\lambda_1, \lambda_2, \lambda_3\}$

4.2 Waves propagation through a stratified atmosphere

The pressure field over a cylinder that surrounds the aircraft has to be used to propagate the signal to the ground. The nonlinear distortions due to the propagation of the disturbances to the ground can be analyzed with the nonlinear acoustic theory and with the acoustic geometry. Two hypothesis must be satisfied in order to apply this approach [15]:
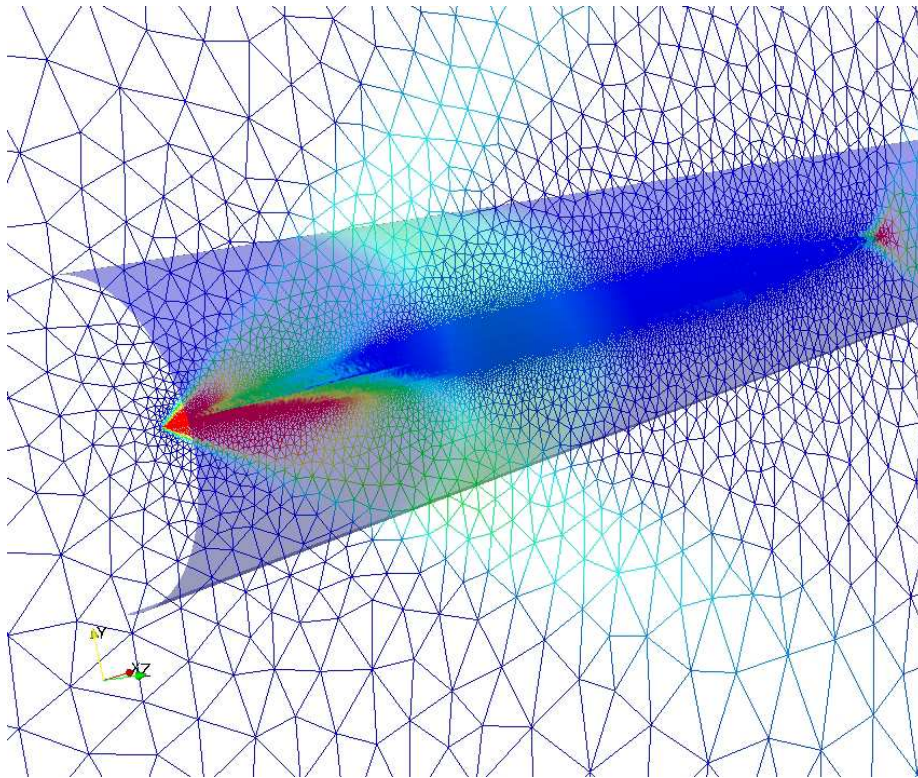
- small perturbations;

Figure 9: Extrapolation of the pressure field over a cylinder with R/L =0.1

- ratio between the perturbation scale and the propagation scale very low.

Before analyzing the ray-tracing approach, it is necessary to introduce the reference systems. We consider a Galilean fixed system $\Re(x, y, z)$, with x directed in the East direction and z directed as the North. In this reference the aircraft is moving in horizontal rectilinear uniform flight. It is possible to consider a reference system $\Re_1(x_1, y_1, z_1)$, in motion with the aircraft and with its origin fixed at the vertex of the fuselage nose and with the direction defined as in figure 10.
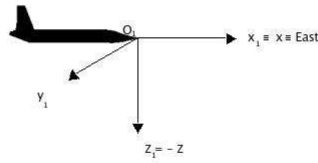
Figure 10: Moving reference system

At each instant of time during a supersonic flight if the fuselage is a slender body a Mach cone has its vertex on the fuselage nose [15]. The main characteristics are that it is tangent to the wave front and the normals at the vertex form a wave normal cone as in figure 11. The half angle of this cone is an angle complementary to the Mach angle μ.
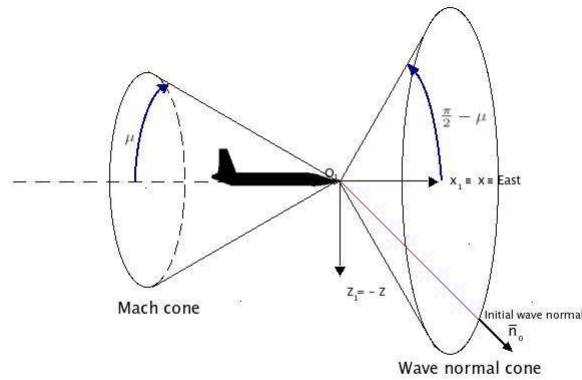

Figure 11: Mach cone and wave normal cone

A wave front propagates at a velocity, called ray-velocity, that is the sum of the local sound speed and the wind velocity in the propagation direction:

$$\mathbf{c} = a\mathbf{n} + \mathbf{u} \cdot \mathbf{n} \tag{19}$$

where **u** is the wind velocity considered equal to zero, and **n** is the normal to the front wave.

In order to define completely an acoustic ray it is necessary to define how change the normal vector along rays.
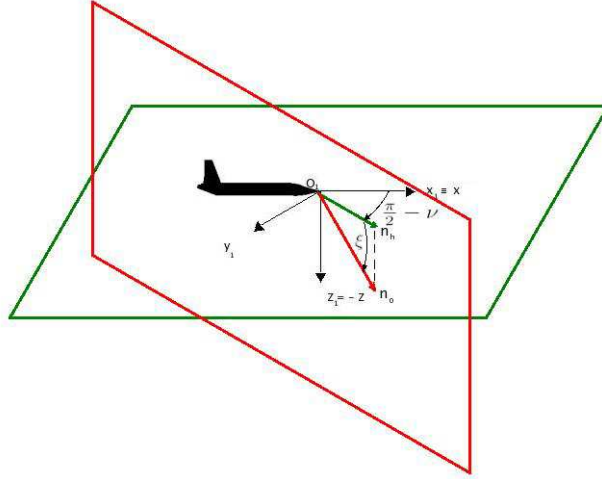

Figure 12: Normal wave angles definition

It is necessary in figure 12 to introduce the angle ξ between the horizontal plane and the wave normal, and the angle $\frac{\pi}{2} - \nu$ between the flight trajectory and the projection of the normal on the horizontal plane. In this way the definition of the propagation direction can be written as:

$$\mathbf{c} = a\cos(\xi)\mathbf{n}_h - a\sin(\xi)\mathbf{z} \tag{20}$$

Using the Snell law as in [14] it is possible to define an invariant quantity on a single ray, but that it changes from a ray to another one. The projection in the initial wave normal $\mathbf{n}_0$ direction of the current propagation velocity is a constant:

$$c_0 = \frac{c}{\cos(\xi)} = \frac{a_0}{\cos(\xi_0)} \tag{21}$$

With equation 21 we can define the evolution of the angle ξ as a function of the altitude:

$$\cos(\xi) = \frac{a(z)}{c_0} = \frac{a(z)}{a_0}\cos(\xi_0) \tag{22}$$

This equation with the propagation velocity in 20 permit to propagate the disturbance to the ground with a ray-tracing method.

The evaluation of the pressure is based on the evaluation of the so called ray tube area. From acoustic geometry, a ray tube is a volume defined by four rays

very close each other, and the cross sectional area of the tube can be evaluated considering the surface of a parallelogram bounded by four adjacent rays.
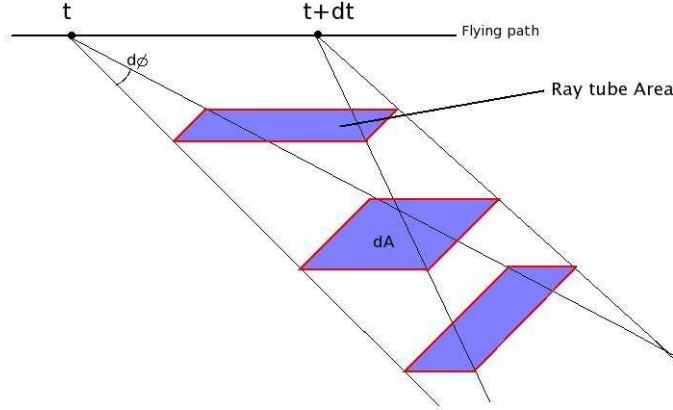

Figure 13: Ray tube area

Essentially the pressure signature on the ground is evaluated using an energetic conservation principle along the ray tube based on the Blokhintsev invariant [14].

The variation of the ray-tube area along the rays express the acoustic signal quantitatively, and it also permits to calculate nonlinear distortions. In fact the invariant, using the ray-tube area; can be written as a function of the Whitham function.

4.3   Ground signature

The result of the disturbances propagation through the atmosphere is presented in this section. In particular the aims is to identify a cylinder R/L that is not too close to the fuselage and that it could avoid a loss of information on the ground.

Figure 14 shows ground signature with different cylinder ratios. The relevant aspect that emerges is that an increase of the R/L value determine a loss of information during the propagation in the CFD field. This is mainly due to a mesh which is not adapted. For the optimization of the fuselage it is possible to consider a low R/L that surrounds the design domain, but in general a fine mesh or an adapted mesh is required. In this research a compromise between the different tools for increase the solution accuracy is used. R/L equal to 0.1 has been selected for this first analysis of coupling the aerodynamic and acoustic problem.
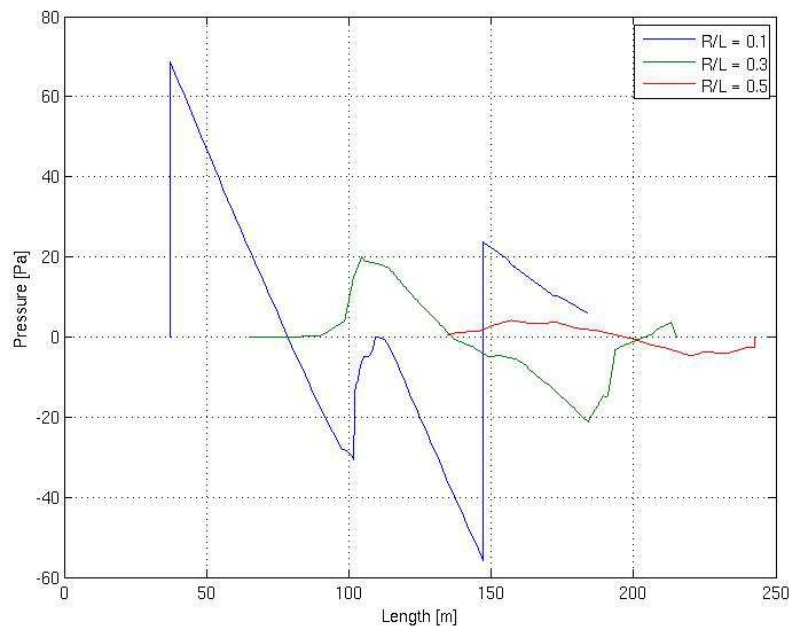
Figure 14: N-shaped wave with different R/L

5   Geometry parametrization and optimization definition

In this first step of the research we have considered to optimize only the geometry of the fuselage of a SSBJ.

The geometry is defined through the use of three meridians represented by Bezier curves. In general a curve could be described using a polynomial defined as:

$$P_n(t) = \sum_{i=0}^{n} a_i t^i \tag{23}$$

where n is the order of the parametrization, t^i is the canonical basis and a^i are the polynomial coefficients. Essentially a Bezier curve is a mathematical formulation of the geometry using a polynomial representation based on Bernstein polynomials. Bezier formulation can be written as:

$$P_n(t) = \sum_{i=0}^{n} B_i^N(t) P^i \tag{24}$$

where $n+1$ is the number of control points and $B_i^N(t)$ is the Bernstein polynomial defined as:

$$B_i^N(t) = C_n^i t^i (1-t)^{n-i} \tag{25}$$

with $i = 0, ..., n$ and $C_n^i = \frac{n!}{i!(n-i)!}$.

The evaluation of the binomial coefficients is numerically instable. Instead using eq. 24 the points that belong to the Bezier curve are evaluated with the De Casteljau algorithm. Starting from the control points P_i and considering the parameter $\tau \in [0, 1]$ the algorithm states as follows

$$\begin{array}{rcl} P_i^r(\tau) & = & (1-\tau)P_i^{r-1}(\tau) + \tau P_{i+1}^{r-1}(\tau) \\ P_i^0(\tau) & = & P_i \end{array} \tag{26}$$

with

$$\begin{cases} r & = & 1, ..., n \\ i & = & 0, ..., n-r \end{cases}$$

The control points for each of the three curves have the same abscissa, in this way it is possible to effectively control the geometry of the corresponding section of fuselage. In fact acting on the z-coordinate of the points belonging to the central meridian by the variable eccentricity it is possible to easily generate non-axial symmetric geometries. Starting from the definition of eccentricity $e = b/a$ the z-coordinate at each point i is defined as $z_i = x_i/e$.

The fuselage is defined starting from the law of areas (Fig.16) and it is axial symmetric, where all sections are therefore circular.

In order to define the initial geometry from the geometric variables, it is necessary to compute a minimization problem between the section surfaces of the guess solution and the ones that respect the linear interpolation of the area law.

The geometric variables are represented by 5 control points for the definition of the nose geometry (Fig.15) and 5 control points for the rear part of the
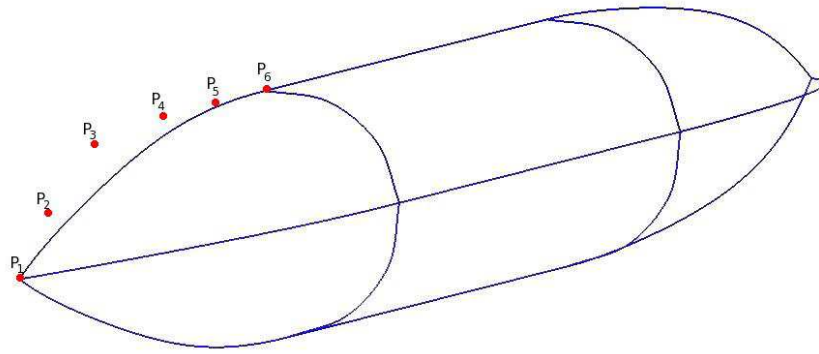
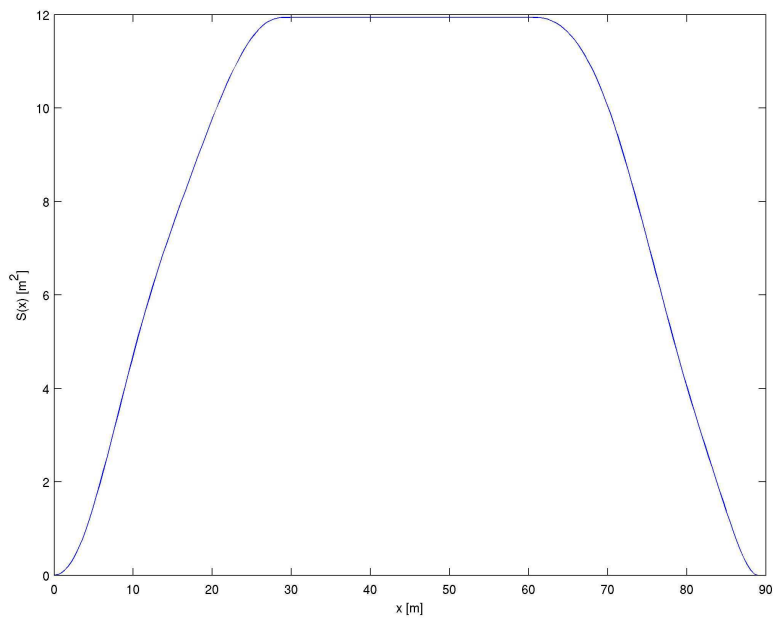Figure 15: Geometry and control points that belong to the optimization variables

Figure 16: Area law for the initial axialsymmetric geometry

fuselage. No other variables are required because the length is fixed and the geometry is axis-symmetric.

$$\mathbf{x} = \left\{ (x, y)^{nose}_{1,..,5}, (x, y)^{rear}_{1,..,5} \right\} \tag{27}$$

$$\min J(\mathbf{x}) = \sum_{i=1}^{n} \left| A_i - \bar{A}_i \right|^2 \tag{28}$$

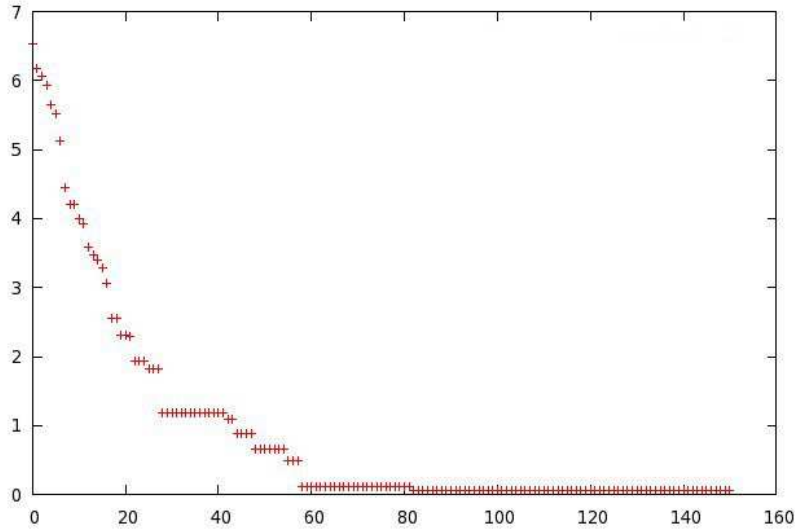where A_i are the guess sections, $\bar{A}_i$ are the interpolated initial surface.

Figure 17: Initial geometry cost function

Figure 17 shows the cost function. After one hundred iterations the evolutionary algorithm reaches convergences to the initial geometry defined by the area law. The accuracy is in order of the 5% with an optimization algorithm based on evolutionary strategies. This method avoid the convergence to local minima due to the initial guess solution. Instead of modify the initial solution, better accuracy could be reached using an increased number of design variables. For our purposes better accuracy is not required, and this choice of variables seems to be a good compromise between computational efficiency and description of the problem.

Gmsh permits to define an unstructured mesh starting from the characteristic length defined at the geometry points. The mesh solver with linear interpolation evaluate the element size everywhere in the computational domain. It appears evident that different mesh complexities lead to very different results.

Before starting the real optimization problem it is necessary to evaluate the accuracy of the signal propagated to the ground. A sensitivity analysis of the signal propagated to the ground has been done in order to evaluate the impact of the different type of mesh. The geometry points as function of their position could belong to three different zone characterized by three different characteristic element lengths:

- fuselage nose

- computational domain boundary

- central and rear fuselage (fixed geometry for optimization)

The following figures show the influence of the variation of the characteristic length over the ground signature and the maximum overpressure. The decrease of the characteristic lengths determine an increase of the number of mesh elements and the convergence to a value for the maximum overpressure except for the value that characterized the central and rear part of the geometry. This aspect is in perfect agreement with physical considerations, in fact these zones do not influence the maximum pressure peak that is due to the fuselage nose. Figure 20(a) shows that this value is not important in our analysis, because it influences the second overpressure peak.

The parameter that influence the maximum overpressure and in this way the optimization criteria is the characteristic length of the nose, while the parameter that influence the number of mesh element is the characteristic length of the tetrahedron that belongs to the computational domain boundary. The optimal choice is to select a characteristic length of the nose small in order to improve the accuracy, while an high value of the computational domain characteristic length could improve the computational performances reducing the number of mesh elements
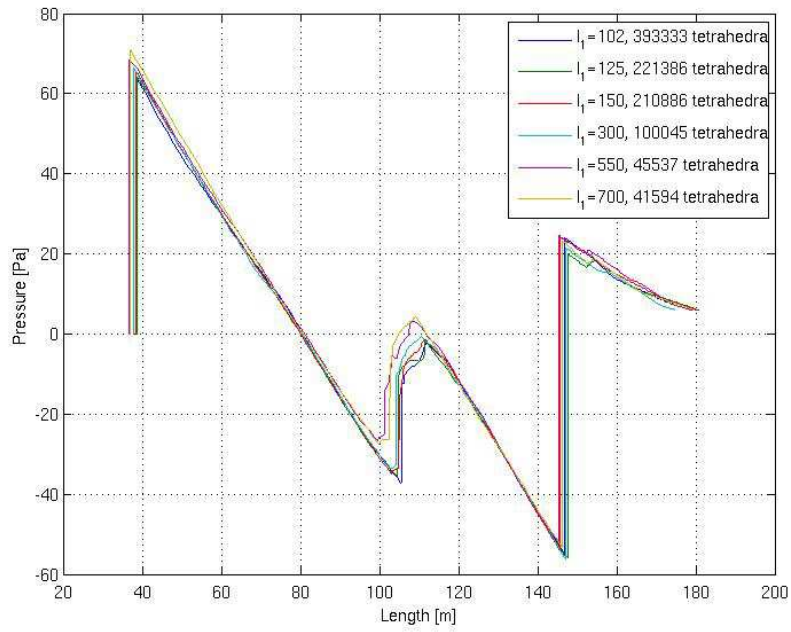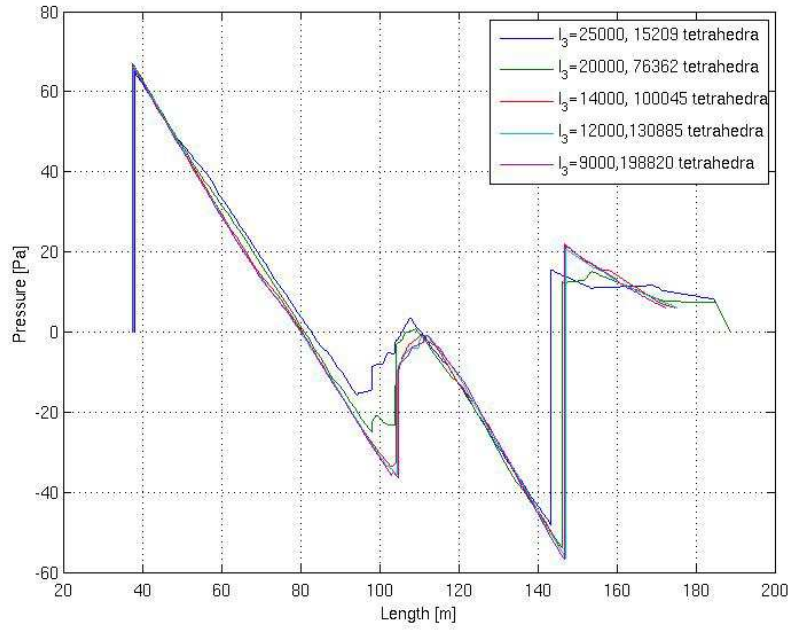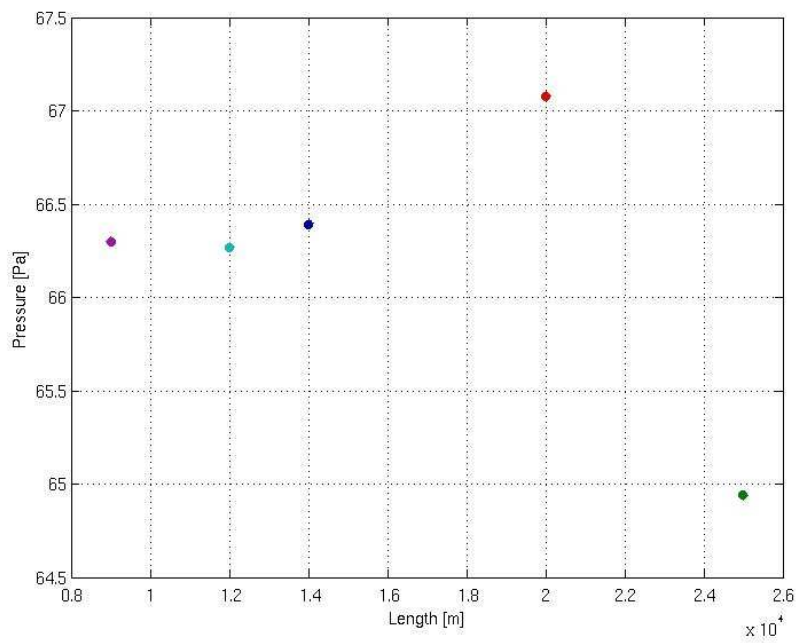
(a) Ground signature
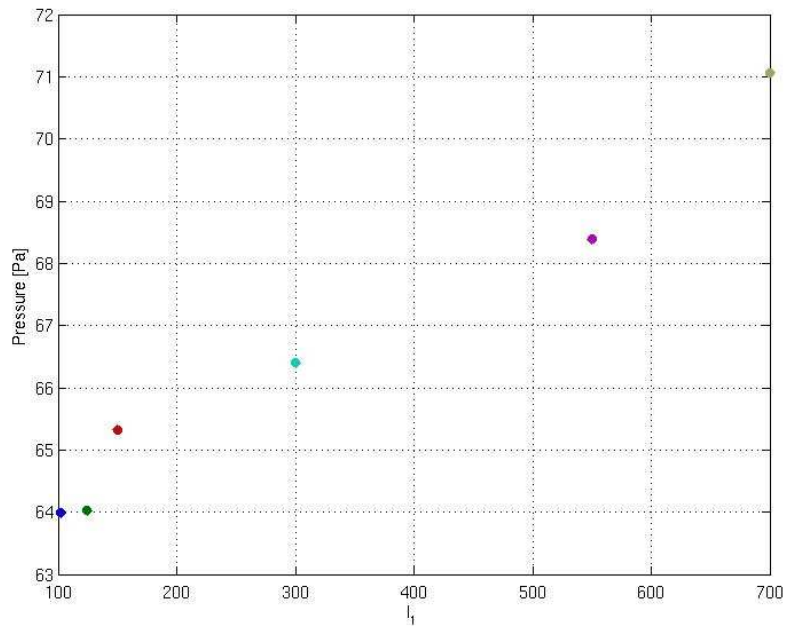
(b) Maximum overpressure

Figure 18: Influence of the nose geometry characteristic mesh length over the ground signature
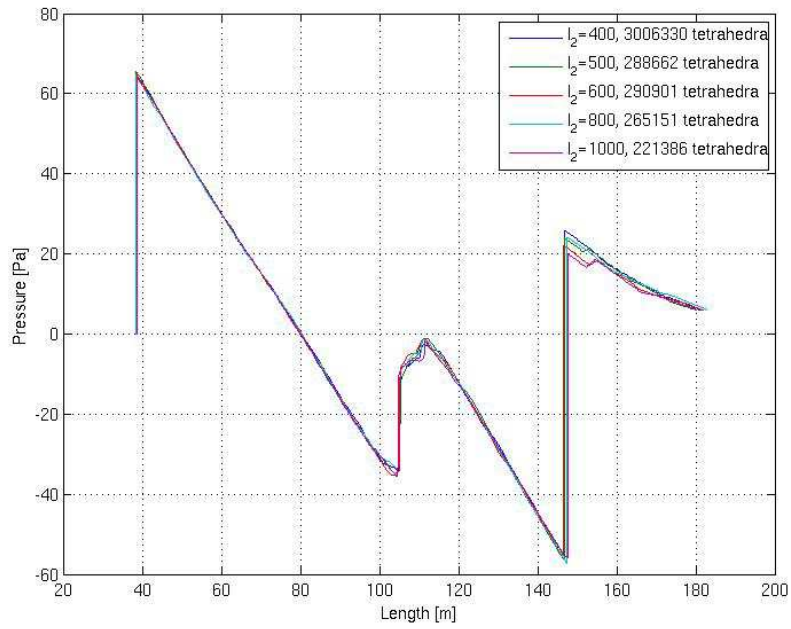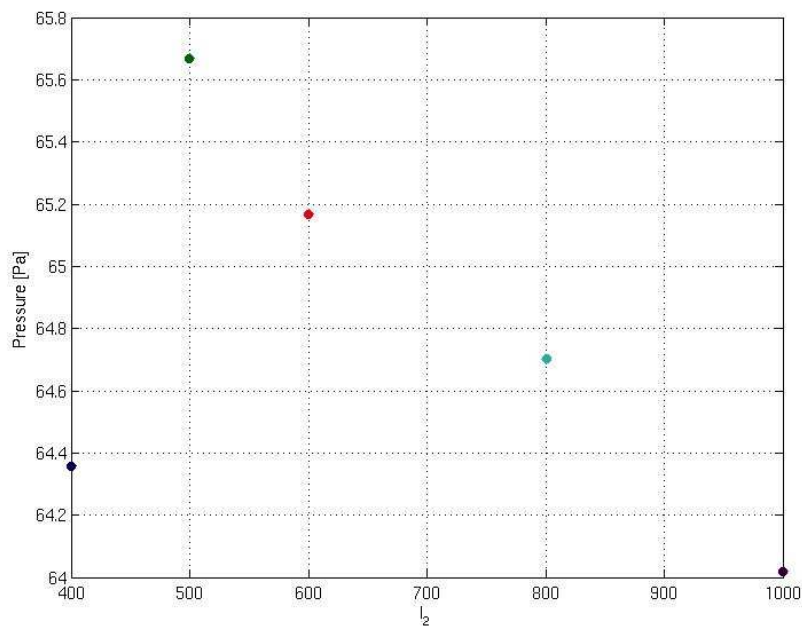
(a) Ground signature

(b) Maximum overpressure

Figure 19: Influence of the computational domain boundary characteristic mesh length over the ground signature

(a) Ground signature

(b) Maximum overpressure

Figure 20: Influence of the central and rear fixed geometry characteristic mesh length over the ground signature

6 Sonic Boom Optimization

The shape design of a SSBJ under the minimization of the sonic boom phenomenon is essentially a multicriteria optimization problem. The reduction of the acoustic criteria has to be attained avoiding an increase of the aerodynamic drag and in this way a degradation of the aircraft efficiency.

Two different strategies could be followed in the optimization loop. The perturbation waves can be propagated to the ground in the optimization algorithm, in this way at each optimization step the ground signature is evaluated. The second solution is to determine apriori a near field target pressure that is the source of a minimized sonic boom on the ground. The first solution is adopted in this research, further research will investigate the influence of this choice in the final solution.

TRAPS, the acoustic propagation code in use at ONERA, permits to perform the propagation efficiently and without high computational efforts.

In figure 21 is shown the global architecture of the optimization loop. The optimization process is coupled with a global mesh regeneration. The accuracy of the regeneration must be not deteriorated by the optimization and at the same time the robustness of the optimization must not be lost with the mesh update. The geometry and the 3D unstructured mesh are generated using the open source software Gmsh [13]. The CFD solution evaluated with the solver Num3Sis is post-processed with a mesh adaptation algorithm. This procedure generates a mesh size map over the entire domain that is used by Gmsh to regenerate a new adapted mesh.

The solution evaluated over an adapted mesh could be used to start the aerodynamic optimization, or as an input for the acoustic propagation. In the last case it is possible to define an aero-acoustic function cost and extrapolate the pressure field over a cylinder that surround the airplane. These steps must be done at each iteration of the optimization loop.

Famosa++ developed at INRIA Sophia Antipolis is an optimization platform in which several optimization algorithm are implemented. These algorithms belongs to the so-called gradient based methods and to the category of Evolutionary algorithm, in this way it is possible to evaluate local and global search and compare the different solutions. This tool permits to analyze multiobjective optimization problems using multiple gradient descent algorithm (MGDA), Nash Game strategies, or Pareto curve using a Pareto Archive Evolutionary Strategies. In the following section brief overviews of the Evolutionary Strategies algorithm and of the steepest descent method are presented in order to define the main steps of these algorithm. An introduction of the Pareto Archive ES is described in order to understand how it works the algorithm.
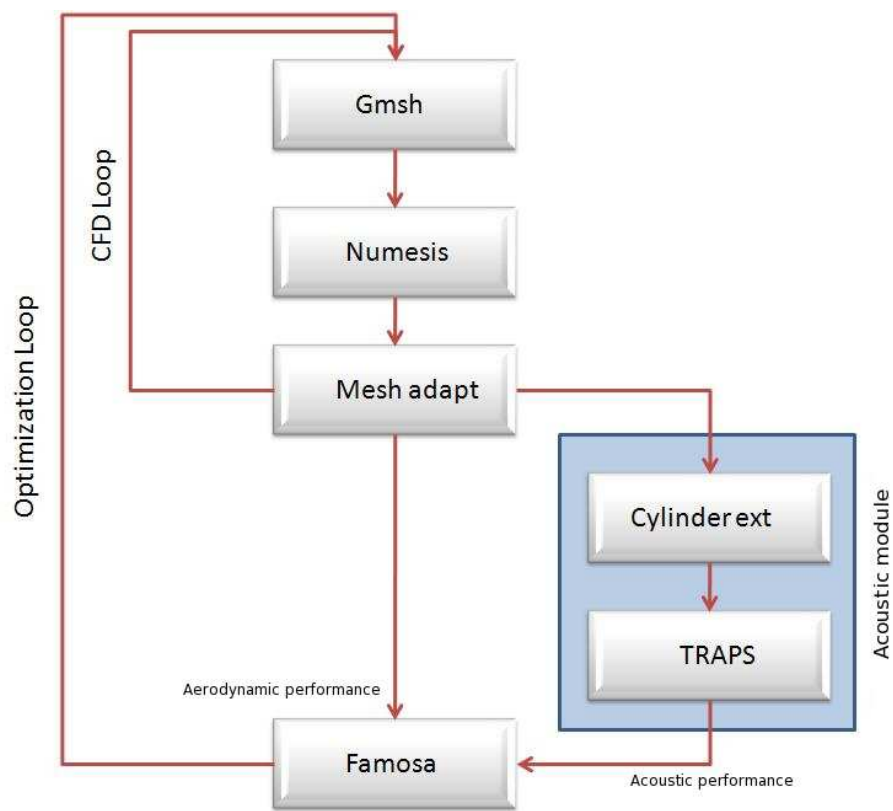
Figure 21: Optimization Loop flowchart

6.1 Steepest descent algorithm

The algorithm used for a local search of the minimum is the steepest descent algorithm. Considering a generic problem $\min f(\mathbf{x})$ with $\mathbf{x} \in \Re^n$.

A direction $\mathbf{d}$ is called a descent direction of f at $\hat{x}$ if there exists $\delta > 0$ such that $f(\hat{x} + \lambda\mathbf{d}) < f(\hat{x}) \forall \lambda \in (0, \delta)$. In particular, if from a Taylor expansion of f($\mathbf{x}$)

$$\nabla f(\hat{x})^T \cdot \mathbf{d} = \lim_{\lambda \to 0^+} \frac{f(\hat{x} + \lambda\mathbf{d}) - f(\hat{x})}{\lambda} < 0 \qquad (29)$$

then $\mathbf{d}$ is a descent direction. The steepest descent algorithm tries to minimize the above inner product moving along the direction $\mathbf{d}$ with $\|\mathbf{d}\| = 1$. Obviously if $\nabla f(\hat{x}) \neq 0$ the direction can be written as

$$\hat{d} = -\frac{\nabla f(\hat{x})}{\| \nabla f(\hat{x}) \|} \qquad (30)$$

where $\hat{d}$ is called the direction of steepest descent at the point $\hat{x}$. This algorithm could be easily implemented as in the following flowchart:
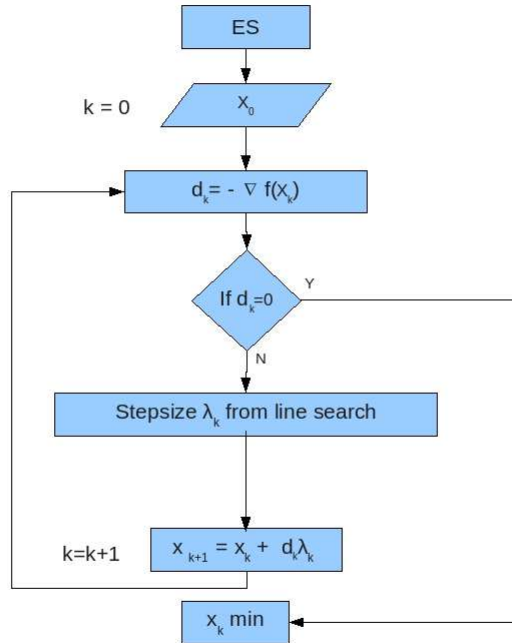

Figure 22: Steepest descent algorithm

6.2 ES algorithm

An evolutionary strategy algorithm is based upon the natural evolution laws. The solver with an iterative loop simulate the generational process with birth and death, variation and natural selection.

Different algorithm has been developed in the category of ES starting from the creation of a single individual for each generation to the multimembered ES in which an entire population is generated at each iteration. The multimembered ES used is the $(\mu, \lambda) - ES$ where μ parents generate λ individuals which undergo selection. Every individuals can survive only for one generation as a difference from the $(\mu + \lambda) - ES$. The algorithm described in a formal way as in [3] is:

$$(\mu, \lambda) - ES = (P^0, \mu, \lambda, m, s, \Delta\sigma, F, g, t) \tag{31}$$

$P^0 =$	population $I = \mathbb{R}^n x \mathbb{R}^n$
$\mu \in \mathbb{N}$	number of parents
$\lambda \in \mathbb{N}$	number of offspring $\lambda > \mu$
$m : I \rightarrow I$	mutation operator
$s : I^\lambda \rightarrow I^\mu$	selection operator
$\tau \in \mathbb{R}$	learning parameter
$F : \mathbb{R}^n \rightarrow \mathbb{R}$	objective function
$\mathbf{g} : \mathbb{R}^n \rightarrow \mathbb{R}$	constraint functions
$t : I^\mu \rightarrow \{0, 1\}$	stopping criterion

The rate of self adaptation depends on the choice of the learning parameter τ. Investigations suggest to choose this parameter proportional to $1/\sqrt{n}$. The mutation operator m act with the hypothesis that small changes are more frequent on every optimization variables a_i and on the standard deviation σ_i.

σ_i is considered as a genetic information of the individual in order to enable self-adaptation of strategic parameters. A random number array with Gaussian distribution between (0,1) is added to the value in order to simulate mutation. The combination with the selection operator s generate individuals with better adjusted parameters that is strictly connected with better performances.

The selection operator s determines the fitter individuals that belong to the next generation, evaluating the value of the objective function and selecting the individuals that minimize it. This iteration process stops when the criteria t is satisfied. This is an arbitrary criteria that could depends on the number of generation, the elapsed time, relative progress between two consecutive generations.

The main step of the algorithm can be written as follows:

- Initial population $P^0(a_i^{0,I})$

- $m(a_i^{0,I}) \Rightarrow (\mathbf{x}^{II}, \sigma^{II})_i = a_i^{0,II}$

- $s(P^0(a_i^{0,II}) \Rightarrow P^I(a_i^1)$

where the mutation step consists in the sequential evaluation of the optimization variables:

$$\sigma^{II} = \sigma^I \exp(\tau \mathbf{N}_O(0, 1)) \tag{32}$$

$$x_i^{II} = x_i^I + \sigma_i \exp \mathbf{N}_{O,i}(0, \mathbf{I}) \tag{33}$$

6.3 Pareto Archive Evolution Strategy

The Pareto Archive Evolution Strategy (PAES) is an algorithm based on ES algorithm, developed for multiobjective problems. In particular the algorithm used in this research is (1+1)-PAES where there are 1 parent and 1 offspring.

A PAES algorithm is mainly composed of three parts: individual generator, candidate evaluation and selection, non-dominated solutions archive. The first two steps are in common with the classical ES algorithm. With mutation, and selection functions at each iteration the algorithm produces a single new individual and maintains the single current solution.

The new aspect is the search for non-dominated solutions. The algorithm create a grid in the objective space in order to define the location of the individuals generated. At each iteration the new individuals is added to the archive if it is not dominated by other solutions and if it belongs to a less crowded region than the current solution, the new candidate becomes the current solution. The current solution represent the individual from which a new individual is generated through mutation.

In other words the algorithm with a local search strategy tries to fill objective space region with a small population of point that are non-dominated.

Following the approach defined in [17] the algorithm follows several steps. At the beginning the starting point is the candidate c that it is added to the archive. A new solution m is then generated with mutation from c and it is evaluated. The evaluation of m consists in several if conditions:

```
If (c dominates m)
   then eliminates m
else if (m dominates c)
       then overwrite c with m and add it to the archive
     else if (m dominates by a point in the archive)
             then eliminates m
             else apply function test(c,m,archive)
```

The comparison with archive population is done by a function test. This function defines also the local search area by the selection of the current solution. The algorithm is defined as follows:

```
If (archive not full)
   then add m to archive
else if (m is in a less crowded region than another archive point)
     then add m and remove a point in a crowded region
If (m is in a less populated area than c)
   then m is the new current solution
else c is the current solution
```

This simple algorithm with a small amount of evaluations can define a well approximated Pareto set. Particular attention requires the parameter that define the discretization of the objective space.

6.4 Problem statement

In this first step of the research we have considered only the optimization of the nose of the fuselage, leaving fixed the central and rear section. The design

variable of optimization are represented by the control points of the Bezier curve and by the eccentricity law along the axis of the fuselage. In this way it is possible to consider also non-axisymmetric geometry. The eccentricity law is defined as a piece-wise continuous function:

$$e(x) = \begin{cases} \frac{1-e_0}{x_{ecc}} + e_0, & x < x_{ecc} \\ 1, & x \geq x_{ecc} \end{cases} \tag{34}$$

where the optimization parameters are the initial eccentricity e_0 and the abscissa along the fuselage axis x_{ecc}.

The optimization variables are $\mathbf{x}$ and the geometry variable $\mathbf{y(x)}$. The array $\mathbf{y(x)}$ contains the control points of the half and bottom meridian.

The x-coordinate of each point P_i that belongs to $\mathbf{x}$ define the fuselage section, while the y-coordinate and the eccentricity $e(x_i)$ identify a unique shape for the fuselage nose.

The main step consists in the definition of a valuable functional cost to be minimized. The ultimate goal is to obtain an optimized shape of the fuselage nose that minimizes the sonic boom, trying not to degrade the aerodynamic efficiency. The first functional is aerodynamic type only and is established as usual in the coefficient of drag. In [2] the cost functional be minimized is the deviation between the ground pressure signature and a target one.

Other criteria may be based on reducing the harmful effects on man, [15] adopted a policy that is based on amplitude and time separation between two physically distinct shocks, but at auditory level perceived as a single event.

In this research we chose to minimize the magnitude of the initial shock generated at the forward fuselage and propagated to the ground. This appears to be a compromise between computational simplicity, results accuracy and consistency with the problem analysis.

This objective has been also suggested by DARPA for the Quiet Supersonic Platform program (QSP) [9].

6.5   Flow around the fuselage and acoustic propagation

In this section the ground signature for the initial geometry is presented. The flight conditions for the test case considered are the following: $M_\infty = 1.8$, $P_\infty = 1, \gamma = 1.4$, $\alpha = 2^o$, $h = 15000$ m.

Figures 23 and 24 show the pressure field on the nose of the fuselage and the Mach cones along the initial geometry

The shock on the bottom part of the fuselage will be propagated through the atmosphere is the strongest and has to be minimized with the optimisation loop in order to reduce the ground signature.
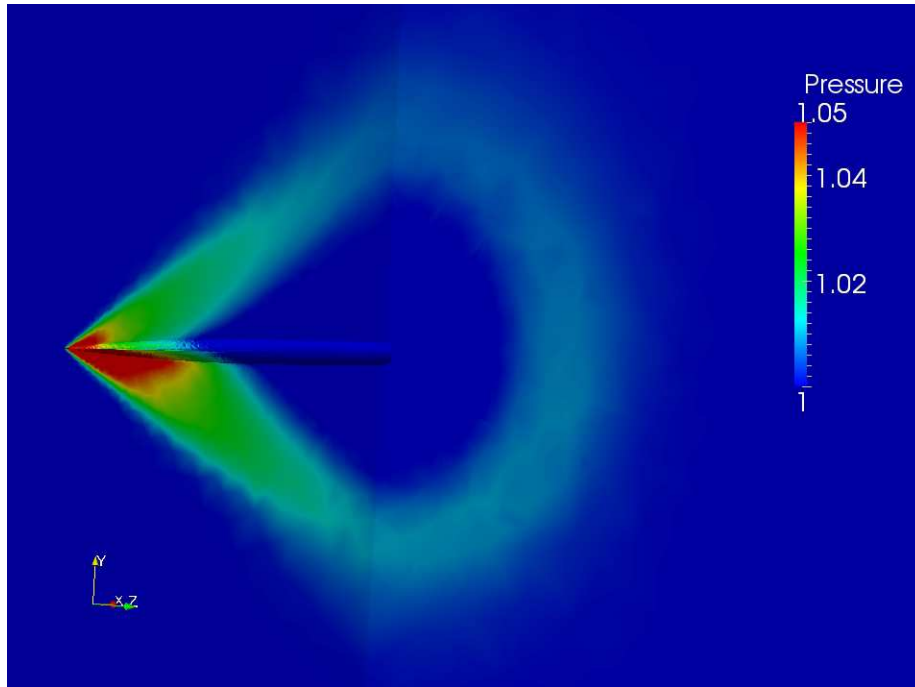
Figure 23: Nose pressure field. Initial geometry non adapted unstructured mesh with 570000 elements
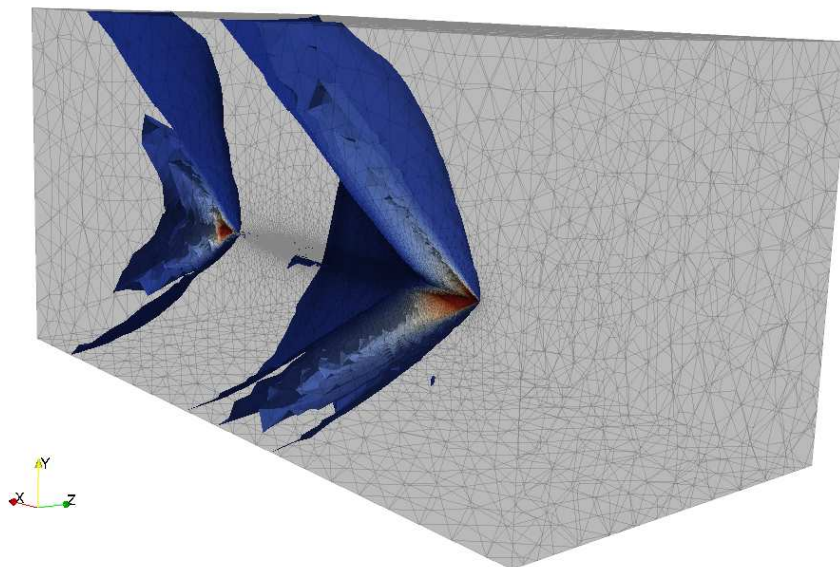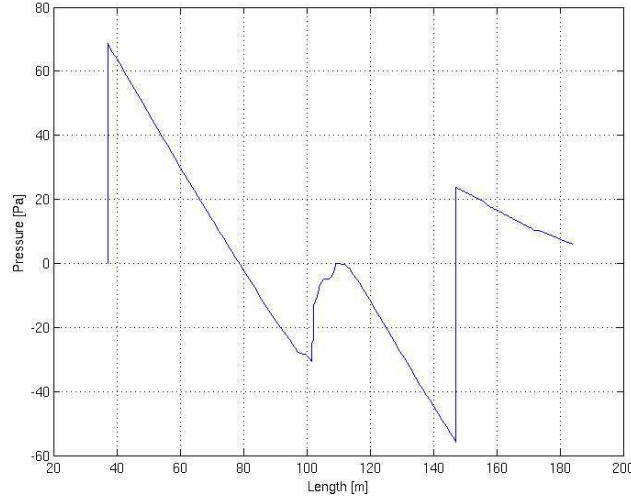

Figure 24: Mach cones initial geometry

Figure 25: Ground signature initial geometry with R/L=0.1

6.6 Optimization results

We want to compare three different configurations than the initial geometry according to the functional considered: Low Drag, Low Boom and bi-criteria that consists in a aero-acoustic optimization. The solutions for the mono-criteria optimizations are obtained using the hybrid algorithm where the optimal solution of the evolutionary strategy has been used as a starting point for a steepest descent algorithm. In this way it is possible to join together the advantage of a global search method at the beginning of the optimization and the gradient based algorithm local search performances in the neighborhood of the global minimum. The first configuration consist in a classic optimization problem that aims to minimize the fuselage drag. The functional for the low drag configuration is:

$$J_{AERO} = C_D \tag{35}$$

No constraints are required because the fixed rear part of the fuselage impose geometric constraints on the nose.

Different objective could be selected for the acoustic functional to be minimized. It is outside the goals of this first phase identify the influence of the functional on the final configuration. We have adopted the maximum overpressure peak of the ground signature as a cost to be minimized:

$$J_{ACOUS} = \max \Delta p_+ \tag{36}$$

The aero-acoustic optimization has been evaluated using the PAES algorithm (see section 6.3) and the adaptive sum method for multiobjective optimization (AWSM) in order to compare the different Pareto front.

The AWSM tries to minimize a functional defined as

$$J = \frac{\alpha_1}{sf_1} J_{AERO} + \frac{\alpha_2}{sf_2} J_{ACOUS} \tag{37}$$

where α_i are weights and sf_i are scaling factors.

It is an apriori method for evaluating a Pareto set[18]. If all of the weights are positive, as assumed in this study, then the minimization of the functional provides a sufficient condition for Pareto optimality.

The values of the drag coefficient and of the maximum pressure peak are shown in the table below:

Configuration	C_D	Max overpressure [Pa]
Initial	78490.51	68.79
Low C_D	69565.99	69.22
Low boom	280707.91	45.75

Considering the mono-criteria aerodynamic optimization it is possible to state that the parametrization adopted, despite simplicity, it allows a reduction of 12% of the drag coefficient.

Figure 26 shows the convergence of the functional J_{AERO} respect to the iterations number with an evolutionary strategy. This result shows that the initial point of the steepest descent algorithm is near to the final value. In fact the gradient based algorithm reduce the functional only by the 2% of the initial value.

Figure 27 shows the pressure field around the nose for the low drag configuration, the magnitude of the shock zone in the zone below the nose is reduced and the shock is more diffused.
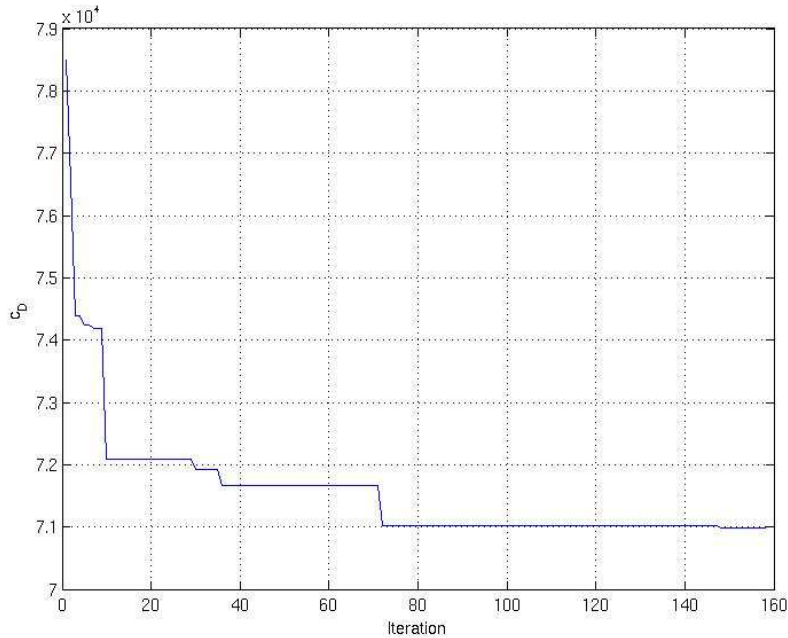

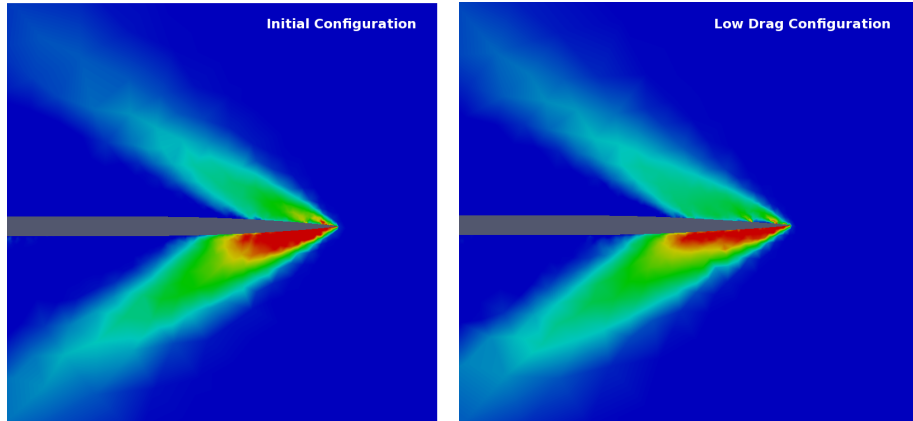Figure 26: Aerodynamic optimization of the fuselage nose. Cost function for ES algorithm

Figure 27: Low Drag configuration

The results of the mono-criteria acoustic optimization are shown in figure 28 and 29. The configuration reduce by the 20% the overpressure shock by creating a secondary peak of equal magnitude. This is due to an unconventional configuration. The nose is thin and the central is a truncated cone because the rear is fixed. This configuration in practice is not acceptable because it is required a minimum internal volume size and because of the high value of aerodynamic resistance that degrades the efficiency dramatically.
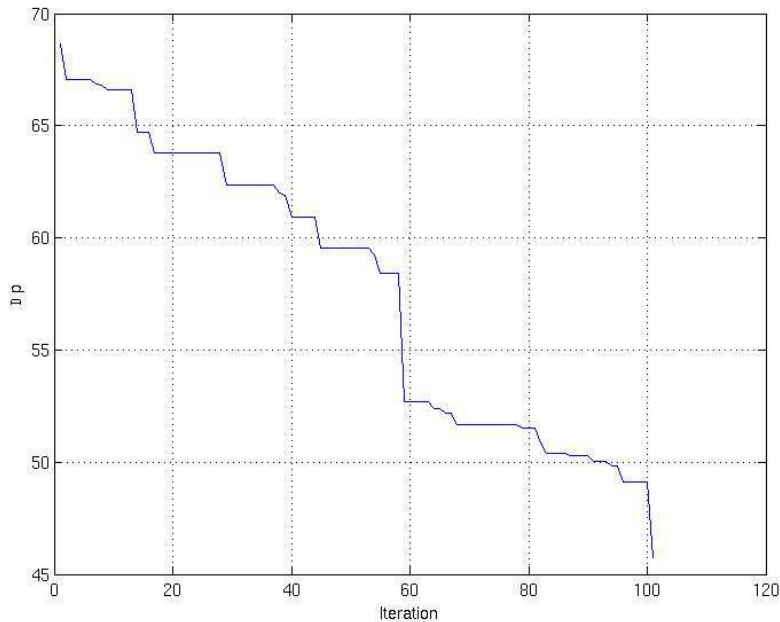
Figure 28: Sonic boom maximum overpressure minimization. Cost function for ES algorithm
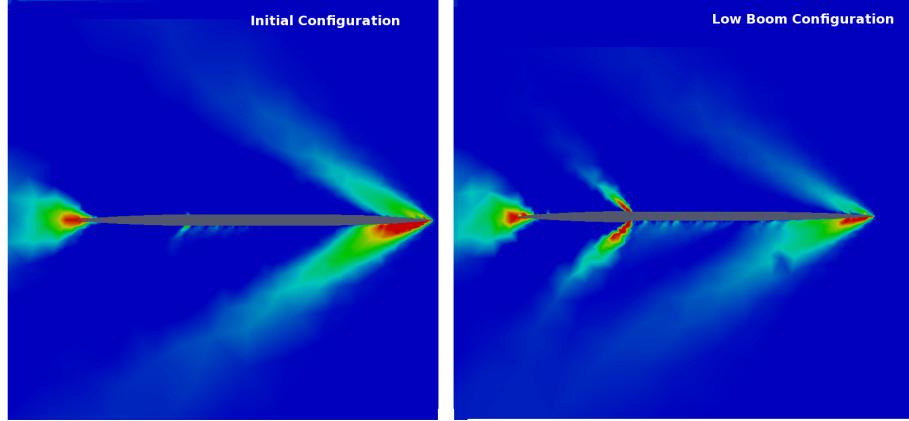
Figure 29: Low Boom configuration

In the table below are presented the values of the optimization variables for the three different configurations:

Configuration	Initial	Low C_D	Low boom
x(P_1)	105000	105078.4	104913.56
y(P_1)	50000	49988.06	50173.36
x(P_2)	109999.7	110201.4	110101.59
y(P_2)	50628.26	50599.44	50747.75
x(P_3)	115037.56	115024.48	115090.11
y(P_3)	50821.29	50555.51	50823.06
x(P_4)	119954.53	119892.89	119960.86
y(P_4)	51210.45	51169.27	51102.63
x(P_5)	124880.7	124964.73	124963.80
y(P_5)	51337.34	51271.6	51168.04
x(P_6)	133897.32	134178.13	133908.86
y(P_6)	51373.79	51382.24	51291.81
e	1	1	1
x_{ecc}	130000	129919.3	130056.24

The ground signature for the three different configurations is shown in figure 30. The initial and the low boom configurations have approximately the same ground signature with an equal overpressure peak. In fact the initial configuration is not so far from the low drag c_D value. The low-boom ground signature is extremely different. Instead of one overpressure peak there are two equal shock. The second pressure peak is due to the shock between the central and the fixed rear part of the fuselage. As already noted this configuration at the aerodynamic performances level is not feasible.

It is necessary to consider a compromise between the two disciplines through a multiobjective optimization.

The aero-acoustic optimization does not have a unique solution. Typically there are many Pareto optimal (PO) solutions that are defined as: $\mathbf{x}^* \in \Omega$, where Ω is the research space, is Pareto optimal if $\exists \mathbf{x} \in \Omega$ such that $f_i(\mathbf{x}) \le f_i(\mathbf{x}^*) \forall i$ and $f_j(\mathbf{x}) < f_j(\mathbf{x}^*)$ for at least one j where f_i are the different objectives.
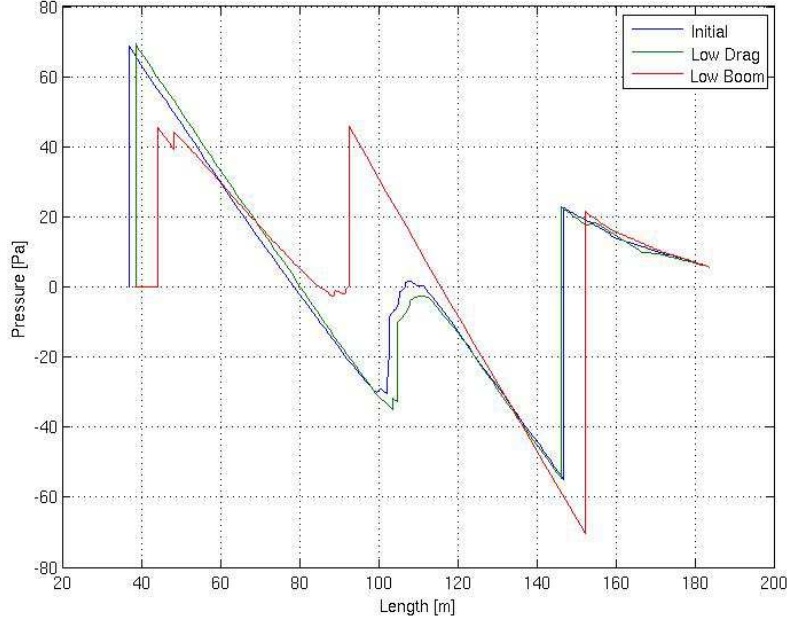
Figure 30: Ground signature in the different configurations

PAES described in brief in section 6.3 evaluate the Pareto optimal set of points represented in figure 31.

In the description of the algorithm we have stated that the discretization step is a critical parameter. An high step value allows a better global research, but with little accuracy locally. To improve the accuracy at the local level the solution adopted is to carry out new iterations of the PAES algorithm starting from initial points belonging to the Pareto front shown in figure 31. In this research as initial solutions four points equally distributed along the front were chosen and a step discretization four times lower than that of single-PAES.

The Pareto front obtained with the multiple PAES (see figure 32) is much more accurate locally, maintaining good local distribution.

The multiple algorithm developed is efficient in the detection of the front and the advantage is that a parallel use can maintain the computational time.

The classical method used to evaluate the Pareto optimal points is the weighted sum method. Considering the functional used for AWSM, the weights affect the solution and there are no fundamental guidelines for selecting them. The approach used in [18] has been used to develop an adaptive weighted sum method.

The weights represents the gradient of J with respect to the different functional:

$$\nabla J = \left\{ \frac{\partial J}{\partial J_{AERO}}, \frac{\partial J}{\partial J_{ACOUS}} \right\}^T = \left\{ \frac{\alpha_1}{sf_1}, \frac{\alpha_2}{sf_2} \right\}^T = \{a_1, a_2\}^T \qquad (38)$$
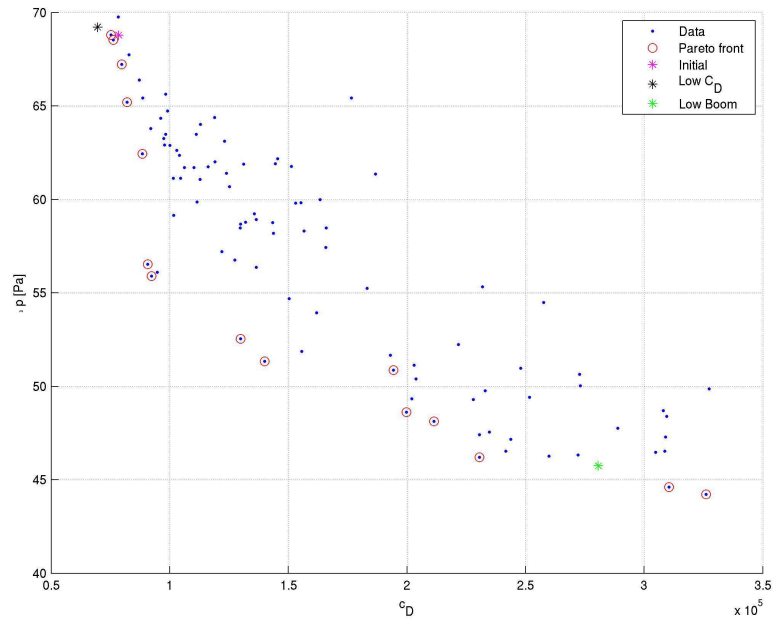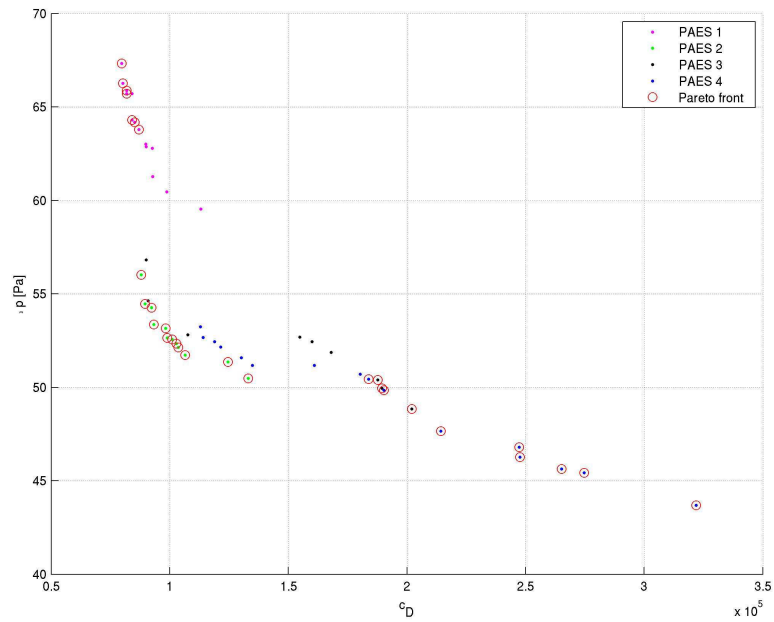
Figure 31: Pareto front PAES algorithm

Figure 32: Pareto front with multiple PAES algorithm

The Pareto optimal solution is found by determining where J-contours are tangent to the Pareto optimal curve. The slope of the Pareto optimal curve is determined as follows:

$$\frac{dJ_{ACOUS}}{dJ_{AERO}} = \frac{a_1}{a_2} \tag{39}$$

The left side of 39 can be approximated as $\Delta J_{ACOUS}/\Delta J_{AERO}$ and assuming $a_1 = 1$ the other weight can be approximated as:

$$a_2 = \frac{\Delta J_{AERO}}{\Delta J_{ACOUS}} \tag{40}$$

Different weights are related to different J-contour and so different search direction for the optimization.

(a) Functional evaluations   (b) Slope of J contours
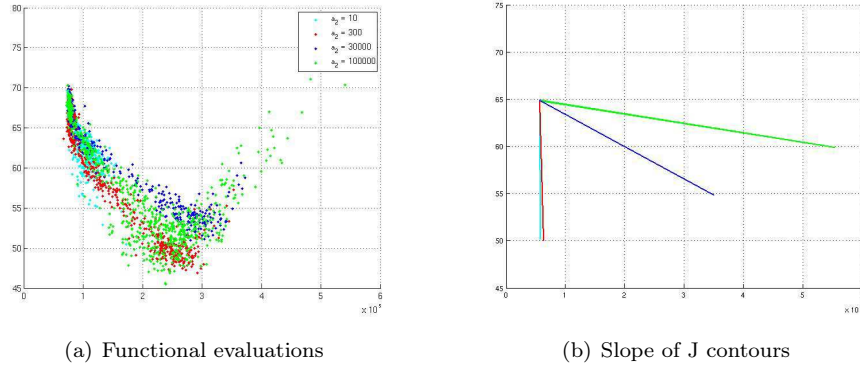
Figure 33: Pareto front evaluation using AWSM

In figure 33(b) are shown the different J-contour normal to the optimum search direction used in our AWSM, while figure 33(a) shows the evolution of the aero-acoustic functional with different weight in order to evaluate the Pareto front. Obviously with four direction we will obtain at convergence only four points which belong to the Pareto curve. Evaluate a large set of points Pareto optimal is really expensive with this method, but a useful approximation consider the other non dominated points as Pareto optimal.

Figure 34 shows the Pareto fronts evaluated with the different algorithms developed, and figure 35 shows the final Pareto front obtained selecting the non dominated points from all the solutions. Among the solutions obtained, great compromises shows reductions of 25% of the sonic boom, with acceptable degradation of aerodynamic performance.

As an example we report a configuration from the Pareto front with the following objective values.

Configuration	C_D	Max overpressure [Pa]
Initial	78490.51	68.79
Bicriteria	92262.27	54.27

The double shocks due to the nose geometry increase the aerodynamic drag, but they create two different overpressure peak. In this way it is possible to
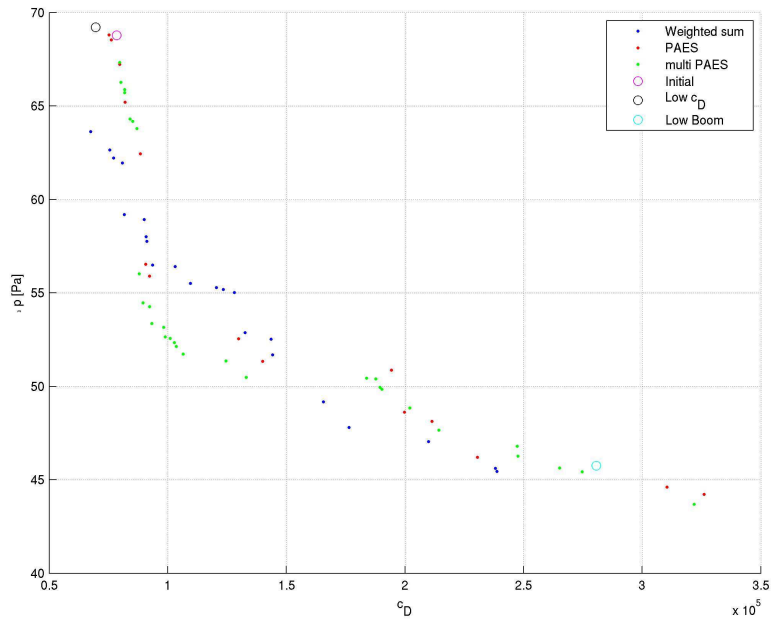
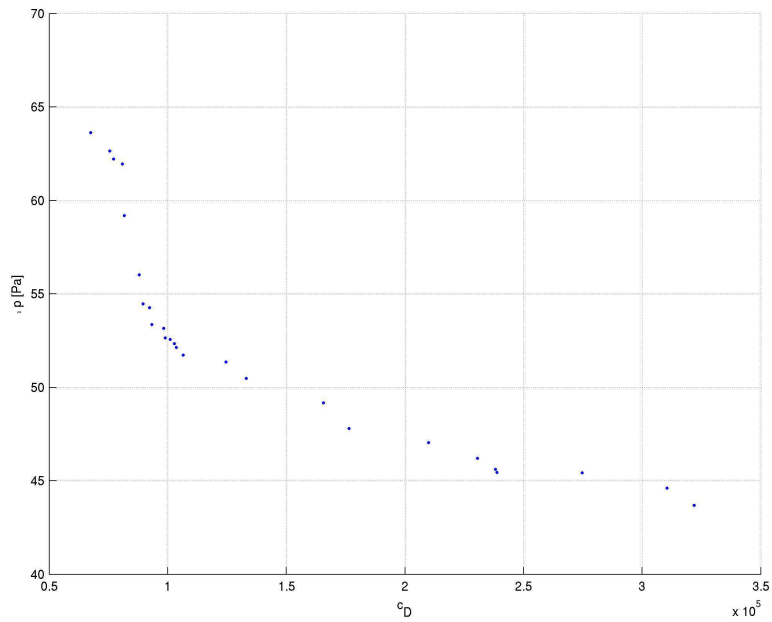Figure 34: Pareto front with different algorithm
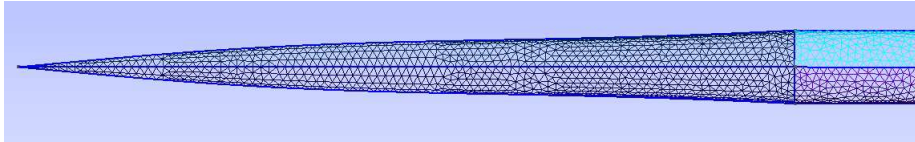

Figure 35: Final Pareto front

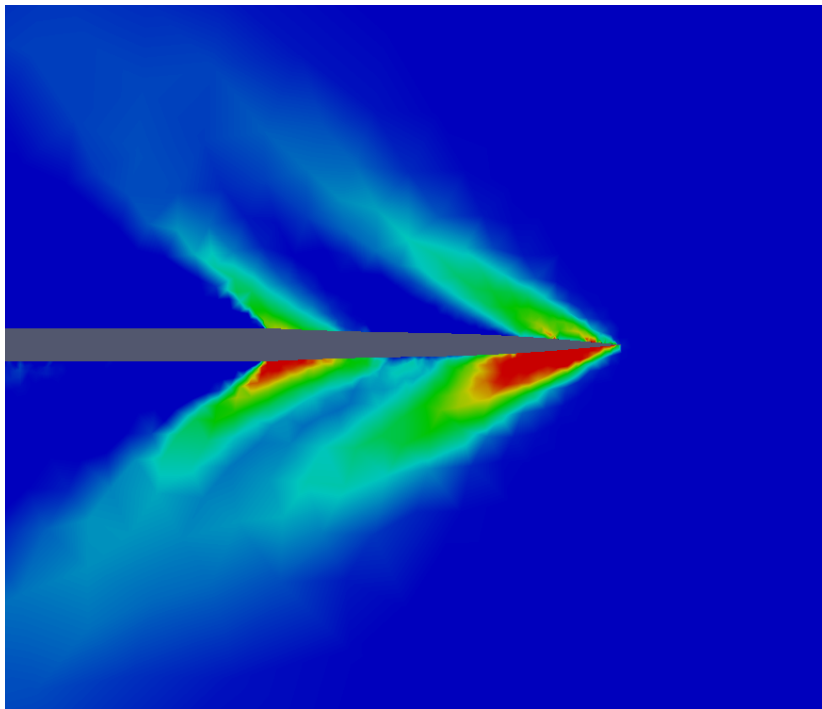Figure 36: Aeroacoustic configuration geometry

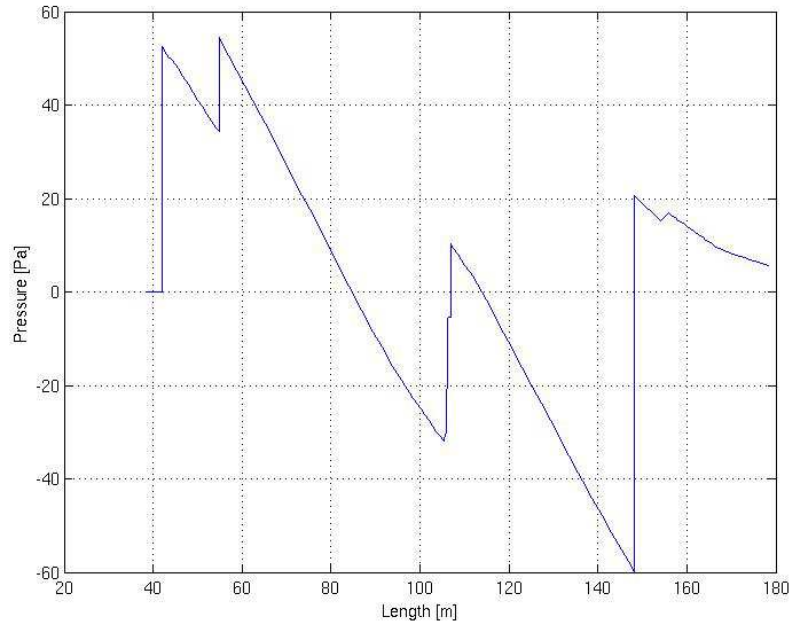Figure 37: Aeroacoustic configuration pressure field

Figure 38: Aeroacoustic configuration ground signature

reduce their magnitude by over the 20%. These two shocks are perceived as separate at the ground because they are separated by an adequate time interval.

The Pareto front identified suffers from three different sources of error. A first error that affects both the aerodynamic and acoustic. This aspect is due to the choice of Euler equations instead of Navier-Stokes equations and is also due to the acoustic propagation model adopted. The second type of error is due to the accuracy of the mesh. The study on the characteristic length in section 5 made it possible to greatly reduce this type of error. Evaluations conducted with mesh of 500000 elements (four times higher than those adopted for the optimization), have led to relative errors on the assessment of the overpressure of 0.3% maximum, and of 10% for the c_D. The third source of error is the order of convergence of the CFD calculation. This error is not very important, because it does not affect the value of Δp nor on the c_D. The magnitude of this relative error is 10^{-5}.

7   Conclusions

This research has enabled the introduction of the necessary elements for analysis of a multi-criteria shape optimization problem. A preliminary optimization problem has been developed in order to take into account 3D CFD computation, sonic boom assesment, and multi objective shape optimization.

The scale diversity between the two different phenomena determine the inefficiency to solve the Euler equations on the whole analysis domain. For this reason it is necessary to adopt the CFD calculation as an input for the acoustic propagation model. The main aspect of this work is the coupling of the CFD solver and the acoustic propagation code in order to define a common optimization algorithm that can takes into account both criteria. Obviously this aspect requires several additional steps or modules.

The identification of the geometry and of the optimization variables determine the final results of the optimization, but also the accuracy of the mesh with the characteristic lengths. Following the Occam's razor principle *entia non sunt multiplicanda praeter necessitatem* (entities must not be multiplied beyond necessity) we have adopted the most simple parametrisation that can define the geometry of the fuselage and an efficient array of optimization variables. The Bézier curve are an excellent and efficient tool that can define complex geometries with a small number of control points, this reducing the dimension of the optimization problem and so the computational time.

The mesh complexity, the physics of the problem and the computational requirements and performances require an additional module that adapt the mesh to the phenomenon analyzed, in particular shock waves.

The procedure developed has allowed to define different configurations. Starting with monocriteria problems we have obtained geometries that minimize the aerodynamic drag or the sonic boom. The choice of the parameter to be used for the reduction of the acoustic disturbances is strictly related to the final configuration. Further research on this topic is required, in particular if we take into account the entire airplane.

A configuration optimized only for a single criteria appears completely inefficient in terms of performances for the other criteria. The next step that we have developed takes into account different algorithm in order to identify the Pareto front for the multiobjective problem.

We have shown in this study that the Pareto Archive Evolutionary Strategy and the weighted sum method methods appropriately tuned for the problem identify with a good approximation the Pareto front. The PAES is efficient to identify the Pareto optimal point with a small number of iterations, but the discretization parameter of the search space is a crucial parameter. With multiple iterations of PAES we have improved the solution joining together a global and local search of the non-dominated points. The weighted sum methods have the same problem of parameter selection and is more computational expensive than the other method. The solutions obtained with the two methods appear similar considering the numerical errors.

Acknowledgements

References

[1] Alauzet F., Mohammadi B. 2003 *Optimisation 3D du nez d'un supersonic business jet basee' sur l'adaptation de maillages.*, INRIA Rapport de recherce

[2] Alauzet F., Sandou S., Daumas L., Dervieux A., Dinh Q. , Kleiveld S., Loseille A., Mesri Y. , Rogè G. 2008 *Multimodel design strategies applied to sonic boom reduction .*, REMN Shape design in aerodynamics 1-20

[3] T. Back, F. Hoffmeister, H. Schwefel 1991 *A Survey of Evolution Strategies*, Morgan Kaufmann.

[4] T. J. Barth, D. C. Jespersen 1989 *The Design and Application of Upwind Schemes on Unstructured Meshes*, AIAA Paper 89-366

[5] P. Batten, N. Clarke, C. Lambert, D. Causon 1997 *On the Choice of Wave Speeds for the HLLC Riemann solver.*, SIAM J. Sci. Comput., 18 1553-1570.

[6] H.G. Beyer, H. Schwefel 2002 *Evolution Strategies*, Natural Computing 1: 3-52.

[7] Busemann A., 1955 *The relation between minimizing drag and noise at supersonic speeds.*, Proceedings of high speed Aerodynamics Polytech Institute of Brooklyn p 133-144

[8] Carrier G., Grenon R., M.C. Le Pape, I. Salah El Din 2009 *Sonic boom prediction in use at ONERA and its application to sensitivity analysis of a supersonic business jet configuration*, AERO '09 Aerodynamics Symposium

[9] Chan M. K. 2003 *Supersonic aircraft optimization for minimizing drag and sonic boom*, PhD Thesis Standford University.

[10] Choi S., Alonso J. J., Weide E. 2004 *Numerical and mesh resolution requirements for accurate sonic boom prediction of complete aircraft configurations*, AIAA paper.

[11] Cheung S.H., Edwards T., Lawrence S. 1990 *Application of CFD to Sonic Boom Near and Mid flow-field prediction*, NASA Technical memorandum

[12] Duvigneau R., Pelletier D. 2006 *A sensitivity equation method for fast evaluation of nearby flows and uncertainty analysis for shape parameters.*, Int. Jo. of Comp. Fl. Vol. 20, No. 7, 497-512

[13] Geuzaine C., Remacle J-F. 2009 *Gmsh Reference Manual*

[14] Hayes W., Haefeli R., Kulsrud H.E. 1969 *Sonic boom propagation in astratified atmosphere, with computer program.* NASA CR-1299

[15] Itham S.E.D., 2004 *Contribution a l'optimisation de la forme aerodinamique d'un avion de transport supersonique en vue de la reduction du bang sonique*, PhD Thesis

[16] Kim K.H., Kim C. 2005 *Accurate, efficient and monotonic numerical methods for multi-dimensional compressible flows. Part II Multi-dimensional limiting process*, Jo. of Comp. Phy. Vol. 208, 570-615

[17] Knowles J.D., Corne D.W. 2000 *Approximating the Nondominated Front Using the Pareto Archived Evolution Strategy*, Evolutionary Computation 149-172

[18] Marler T., Arora J. 2009 *The weigthed sum method for multi-objective optimization: new insights*, Stuct. Multidisc. Optim.

[19] Plotkin K.J. 2002 *State of the art of sonic boom modeling*, Jo. of Acoust. Soc. Am. 111, 530-536

[20] Seebass R. 1998 *History and economics of, and prospect for, commercial supersonic transport*, RTO AVT Course on Fluid dynamics research on supersonic aircraft.

[21] Taylor A. D. 1980 *The Traps sonic boom program*, NOAA Technical Memorandum ERL ARL-87.